Supporting Information

Hierarchical porous polymers via microgel intermediate: green synthesis and applications towards the removal of pollutants

Mohd.Avais and Subrata Chattopadhyay*

Department of Chemistry, Indian Institute of Technology Patna, Bihta, Patna 801106, Bihar, India

** Corresponding authors.*

E-mail addresses: sch@iitp.ac.in

Experimental section

Materials - 1,4-Diaminobutane (99%), 1,8-Diaminooctane (≥ 98.0%), Deuterated dimethyl sulfoxide(DMSO-d^6, 99.9 atom % D) and Deuterium oxide(D_2O, 99.9 atom % D) were purchased from sigma-Aldrich and N,N′-methylene(bis)acrylamide (biSAcrylamide) 3x crystextrapure AR, Iodine, Congo red, Methyl orange, Methylene blue, Rhodamine B (≥ 95%), Lithium bromide, Dimethylformamide(DMF) and n-Hexane were purchased from Sisco Research Laboratories Pvt. Ltd.(SRL). All chemicals were of extrapure or HPLC grade and were used without further purification. HPLC grade water was used for throughout of the experiments.

Synthesis - The poly(amino-amide) porous polymers were synthesized via Aza Michael addition reaction. A generalized procedure is given below. First, N,N′-methylene(bis)acrylamide(MBA) (0.5 g, 3.24 mmol) was suspended in water. The suspension was stirred for at least 5 min at room temperature. After that the required diamine(mole ratio of MBA to di-amine is 2:1) was added to the aqueous suspension of MBA. After addition of the diamine the suspension became clear solution within 5-10 minutes(depends on the type of bisamine used). After a period of time, the clear solution terns milky, indicating the generation of microgels.The milky solution was stirred further until the cosslinked porous polymers were obtained. After that the solvent was removed by free drying to obtain the porous polymer. The freeze dried sample was grinded to obtain a powder sample.

For the characterization of microgels(such as SEC, SEM, TEM, AFM etc) samples are collected from the ongoing reactions in the following time intervals if not otherway maintained.

For MG-1 samples were collected at 2.5 hours and for MG-2, samples were collected at 12 minutes.

Table S1

Samples	N,N′-methylene(bis)acrylamide	Diamines (mmol)	Solvent (mL)	Time of reaction (complete crosslinking)
PP-1	0.5 g (3.24 mmol)	142.5mg (1.62mmol)	Water (5 mL)	3 hours
PP-2	0.5 g (3.24 mmol)	233.5mg (1.62mmol)	Water (5 mL)	20 minutes
PP-2a	0.5 g (3.24 mmol)	233.5mg (1.62mmol)	Water:DMF (3.33mL:1.67mL)	40 minutes

Materials characterizations - Synthesized hyper branched polymers, micro-gel and porous polymer were characterized by using different instruments.

FT-IR Spectroscopy - Fourier transform infrared spectra (FTIR) were recorded in ATR and KBr pellets mode using a Perkin Elmer spectrum 400 FT-IR in the range of 500−4000 cm^{-1}.

Nuclear Magnetic Resonance (NMR) – ^{1}H NMR spectra were measured using a Bruker 400 MHz NMR spectrometers. TMS is used as an internal standard.

Zeta potential & Dynamic Light Scattering (DLS) - The zeta potentials and particle size studies were performed using a Litesizer 500 particle analyzer from Anton paar.

Gel permeation chromatography (GPC) - Molecular weight, poly dispersity index (PDI) and branching of polymers were recorded using size exclusion chromatography (SEC), coupled with a triple detector system. The system contains Shimadzu i-series plus integrated HPLC attached with Refractive index detector (Wyatt Optilab T-rEX), Viscometer detector (Wyatt Visco Star III) and Multi angle light scattering detector (Wyatt DAWN HELEOS LS II). For MG1, DMF (0.01% LiBr was added) was used as the eluent at 45 °C column temperature and flow rate was 0.75 mL/min. THF used as an eluent for MG-2 with same flow rate at 35 °C column temperature. ASTRA 7.3.0 software (Wyatt Technology Corporation) was used for data collection and processing. Berry plot was used for data analysis as it fits best (comparing R^2 value of different fit models – Zimm, Berry and Debye)

Scanning Electron Microscopy (SEM) - Surface morphology of the microgels and porous polymers were studied using a Gemini - 500 Zeiss (Germany) Scanning electron microscopewith energy-dispersive X-ray spectroscopy (EDX). Two drops of the diluted aqueous microgelsolution (collected from the reaction vessel and diluted further to make final concentration ∼8 mg/mL) was dried on a silicon wafer to analyze the morphology of microgels by SEM. For porous polymers, samples were freeze dried before analysis. Prior to analysis, all samples are coated with a thin gold layer.

Transmission electron microscopy (TEM) - Transmission electronic microscope (TEM) micrograms were recorded using JEOL TEM with 200 kV accelerating voltage.

Atomic force microscopy (AFM) – Topography micrograms are taken using atomic force microscope (AFM) (model: Agilent Technologies 5500) in the noncontact mode. Silicon cantilevers having a springconstant of 42 N/m and resonance frequency of 289 kHz are used. To

study the morphology of microgels silicon wafer is spincoated with highly diluted aqueous solutions of microgels(Concentration 0.9 mg/mL).

Brunauer-Emmett-Teller (BET) - Surface area and porosities were measured at 77K and gas absorption studies were performed at 273K using QuantachromeAutosorb iQ2 analyzer. Before experimental setup, HPPs (100– 150 mg) samples were degassed in degassing unit at 110 °C for 5-6 hours with using a 9 mm cell. The Brunauer-Emmett-Teller (BET) isotherm was used to calculate the surface areas and Nonlocal density functional theory (NLDFT) and Barrett-Joyner-Halenda(BJH)method were utilized to calculate porosities of the micro-gel and HPPs. For analysis, MG-1 micro-gels were precipitated by THF. For MG-2 micro-gel was diluted using excess amount of water and the microgels removed immediately via centrifugation. The final product was obtained by vacuum filtration and drying under freeze dried method.

Mercury intrusion porosimetry (MIP) - Meso and macro pores of porous polymers were evaluated by theAutopore IV micromeritics with 414 MPa maximum mercury pressure. To implement the experiment, a freeze dried porous polymer sample was placed in MIP penetrometer, and finally penetrometer was inserted into the equipment port with low pressure.

UV–VIS spectra - UV-vis spectra were measured on Shimadzu UV 2550 Spectrophotometer.

Raman spectra -Raman measurements were performed on a Micro- Raman spectrophotometer (STR 750 RAMAN spectrograph, Seki Technotron Corporation Japan). Raman measurements were done using 633 nm He-Ne laser.

Elemental analysis - Elemental contents of C,N and H were measured using Elementarvario MICRO cube CHNS analyzer.

Adsorption experiments - In this work**,** we calculated the adsorption capacity and efficiency of the prepared porous polymers with different anionic dye like Congo red (CR), methyl orange (MO) and cationic dyes such aS methylene blue (MB) and rhodamine B (RhB). Typically, 10 mg of PPs was added to 10 mL of each dye solutions (concentration 100 to 5000 mg/L). Then the mixture was taken into a 50 mL beaker and stirred with 500−600 rpm rotation at RT until equilibrium was reached. After equilibrium was established (24 hours) 2 mL aliquot was taken from mixture and centrifuged for 10 minute to completely separate the adsorbents. Finally adsorbates concentration was measured by using UV-vis spectrophotometer. The same procedure also applied for iodine adsorption experiment in closed condition.

The adsorption capacity (Q_e) and adsorption efficiency (%) at equilibrium can be calculated by using the following equation respectively.

$$\mathbf{Q_e = [(C_o - C_e) \times V]/ M} \qquad \textbf{……(1)}$$

$$\textbf{Adsorption efficiency (\%)} = \mathbf{[(C_o - C_t)/C_o]\times 100} \qquad \textbf{……(2)}$$

Where C_o and C_e (mg L^{-1}) represent initial and equilibrium concentration of the solute respectively, M (g) is the weight of adsorbent, V is the total volume of solution in liter.

Figures and Tables

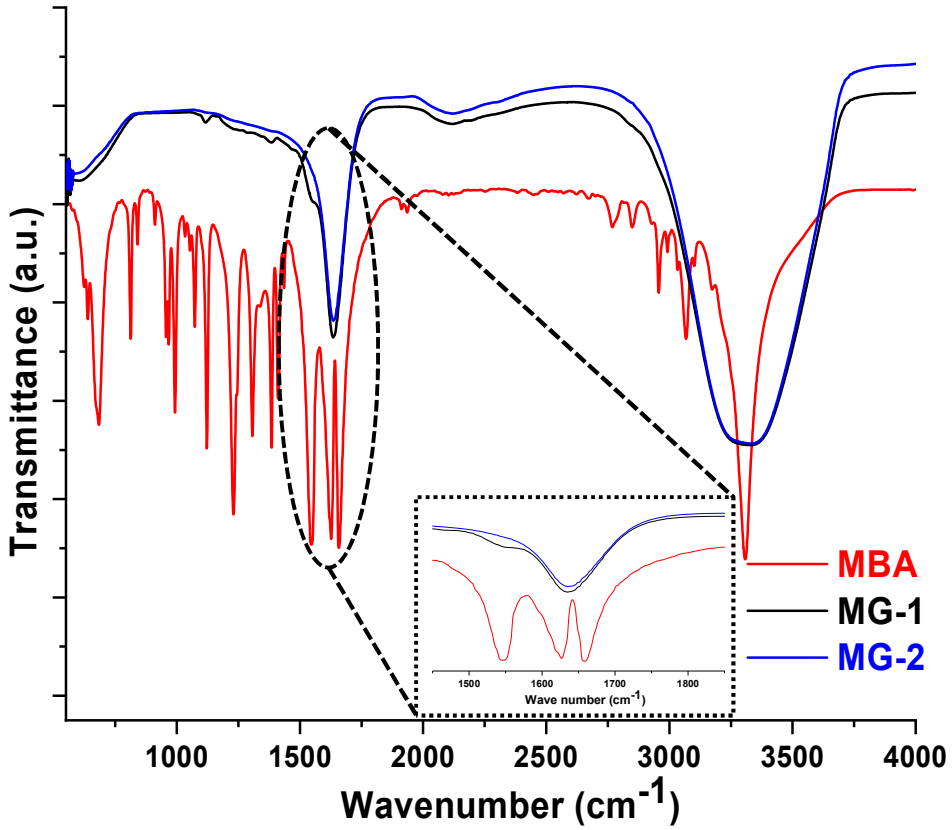

Figure S1: IR spectra of the different micro-gel MG-1 and MG-2 samples in ATR mode

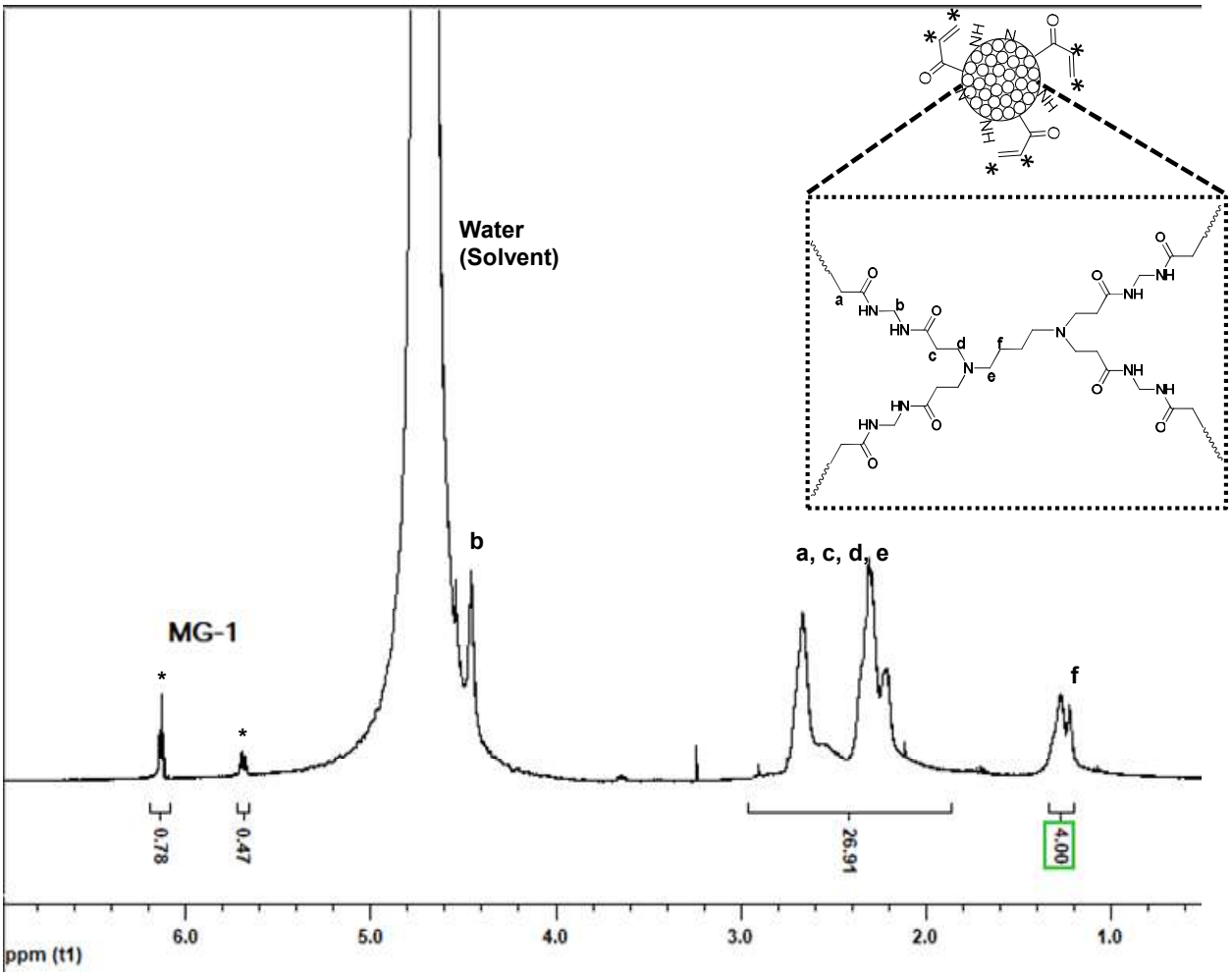

Figure S2: ^{1}H NMR spectrum of MG-1

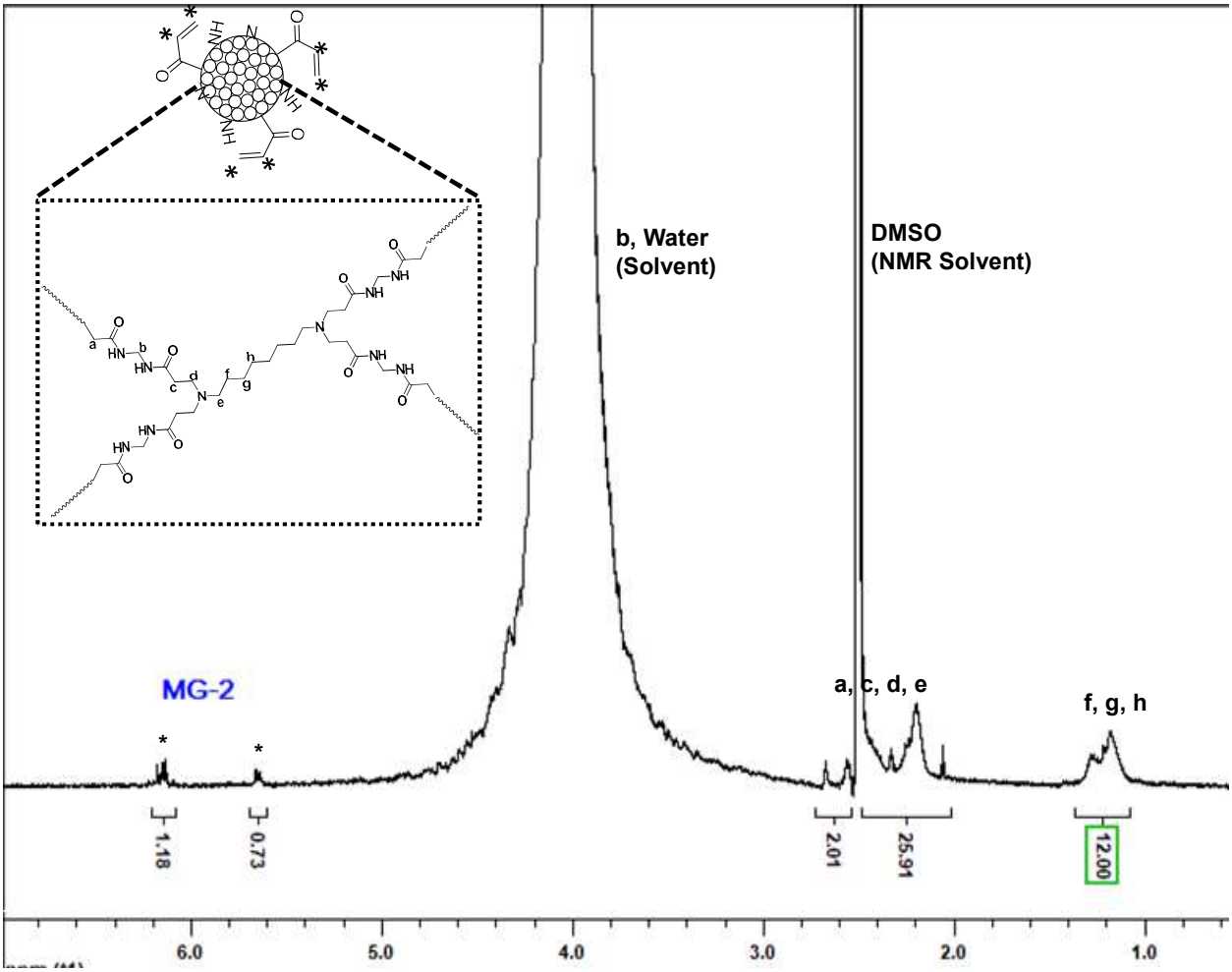

Figure S3: ^{1}H NMR spectrum of MG-2

Table S2 Results of the SEC (coupled with triple detectors) analysis of the Microgels (analysis performed byASTRA 7.3.0 software -Wyatt Technology Corporation)

Samples	M_n(g/mol)	M_w (g/mol)	PDI (M_w/M_n)	rh(v)z (nm)	Rz (RMS) (nm)	Exponent of Mark Houwink plot	Exponent of Conformation plot
MG-1	2.174×10^7	4.863×10^7	2.237	119.2	83.3	0.323	0.41
MG-2	2.631×10^7	8.349×10^7	3.174	285.1	73.4	0.112	0.01*

* abnormal due to microgel-columninteraction/bigger size.

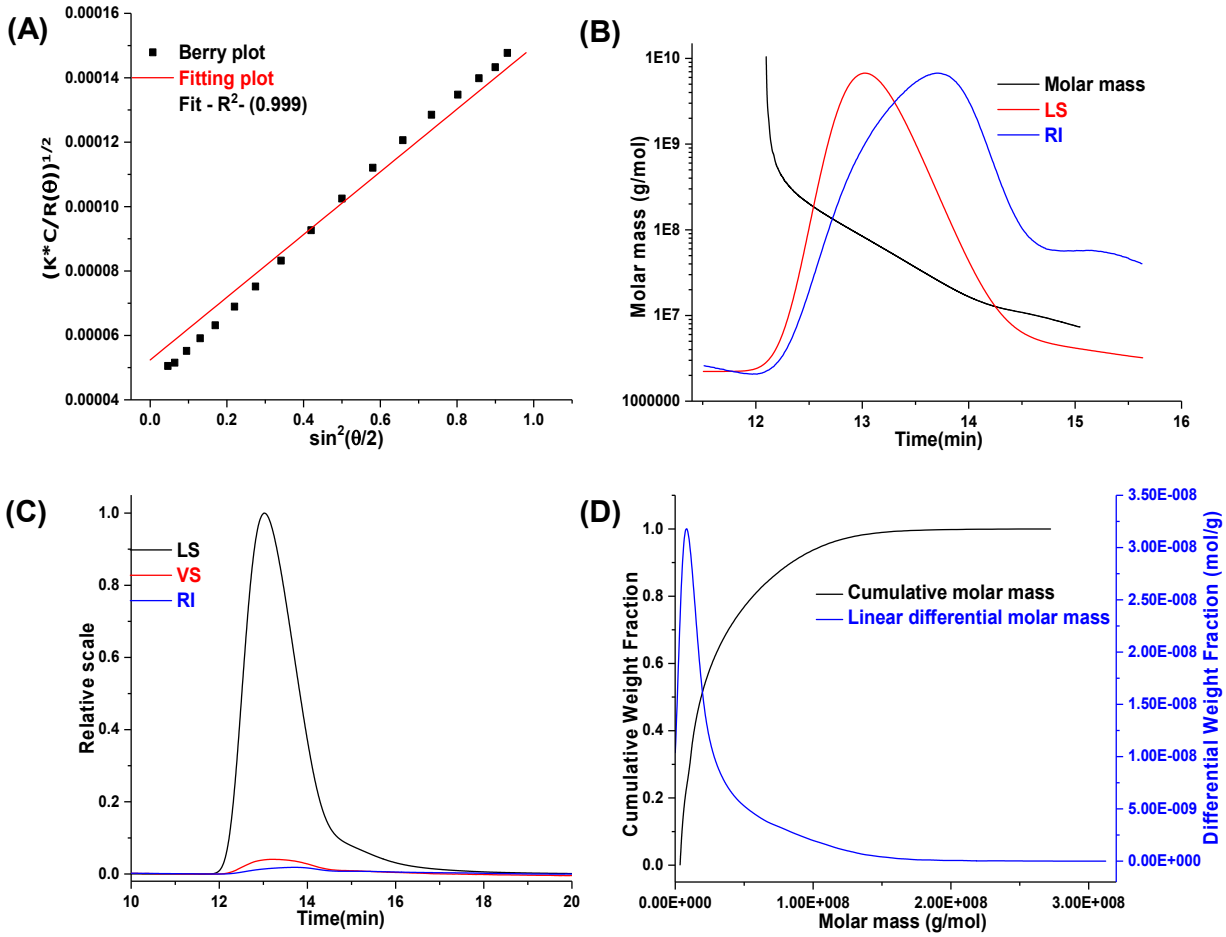

Figure S4: SEC analysis of MG-1 with (A) Berry plot (B) results fitting graph of molar mass versus retention time (C) chromatograms with LS, VS and RI detectors (D) Cumulative weight and molar mass distribution of MG-1

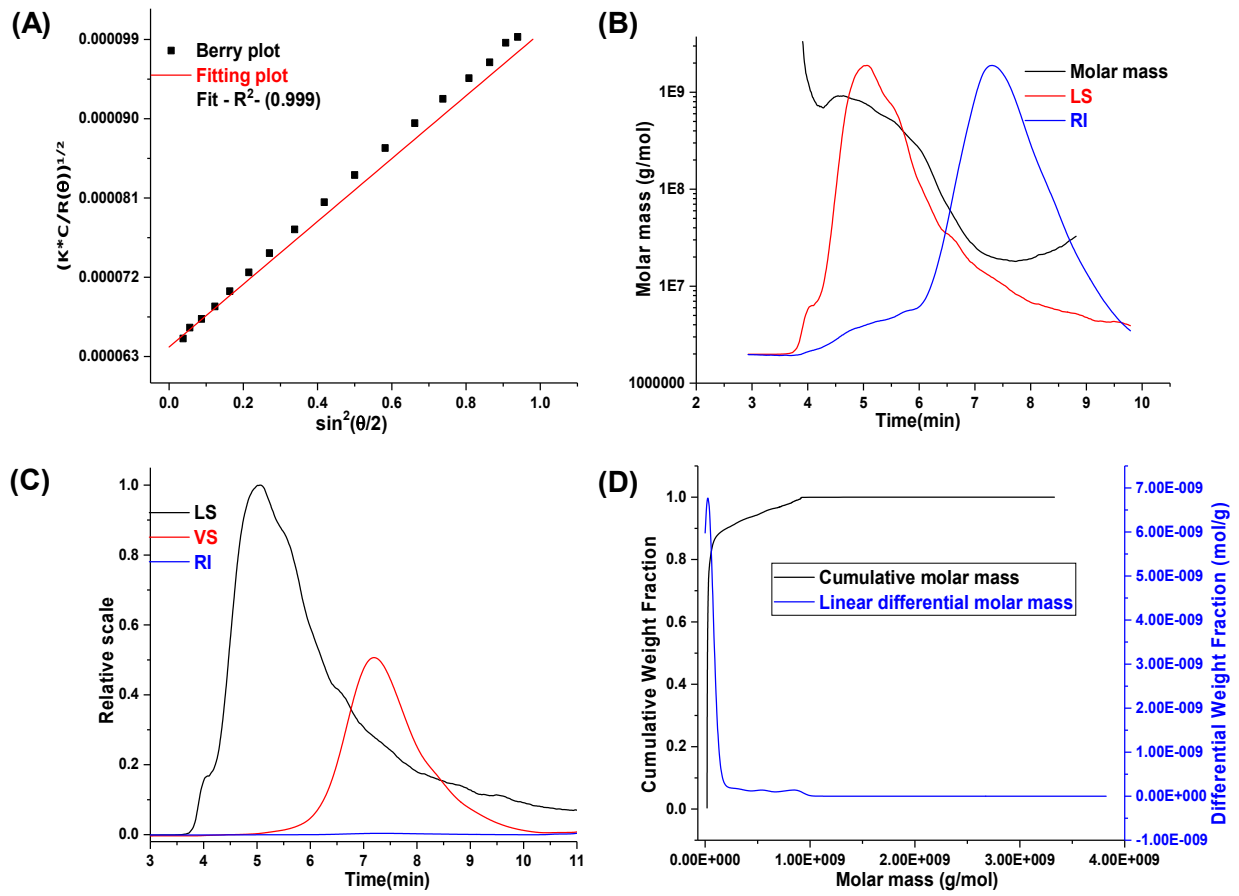

Figure S5: SEC analysis of MG-2 with (A) Berry plot (B) results fitting graph of molar mass versus retention time (C) chromatograms with LS, VS and RI detectors (D) Cumulative weight and molar mass distribution of MG-2

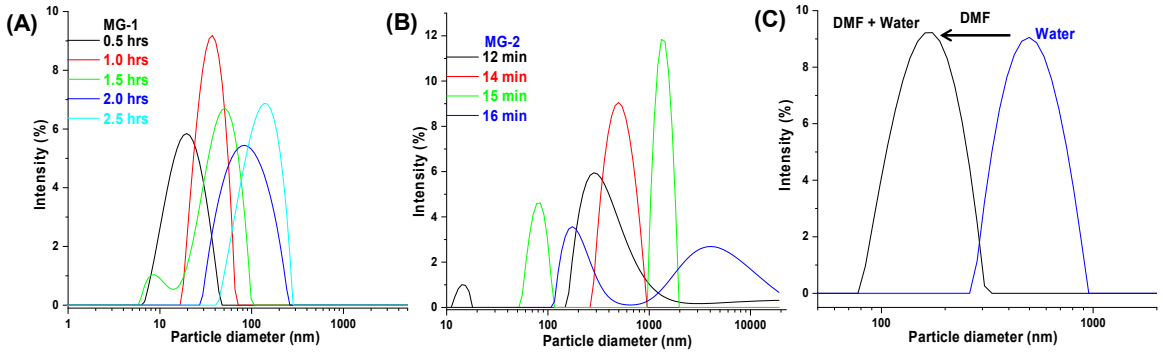

Figure S6: DLS study of (A)MG-1 and (B)MG-2 at different time interval and (C) DLS study of MG-2 in water and DMF:water solution (MG-2 solution was collected after 14 minutes of reaction for analysis)

Based on this analysis the samples were taken (MG-1: 2.5 hours and MG-2: 12 minutes) for details analysis.

Table S3 Particle size analysis at different time interval for MG-1

Time (hrs)	Diameter (nm)	Polydispersity index (PDI)
0.5	20.53	0.229
1.0	37.90	0.223
1.5	41.55	0.261
2.0	81.37	0.235
2.5	131.53	0.256

Table S4 Particle size analysis at different time interval for MG-2

Time (min)	Diameter (nm)	Polydispersity index (PDI)
12	331.67	0.0645
14	499.63	0.197
15	915.03	Multimodal distribution
16	1082.51	Multimodal distribution

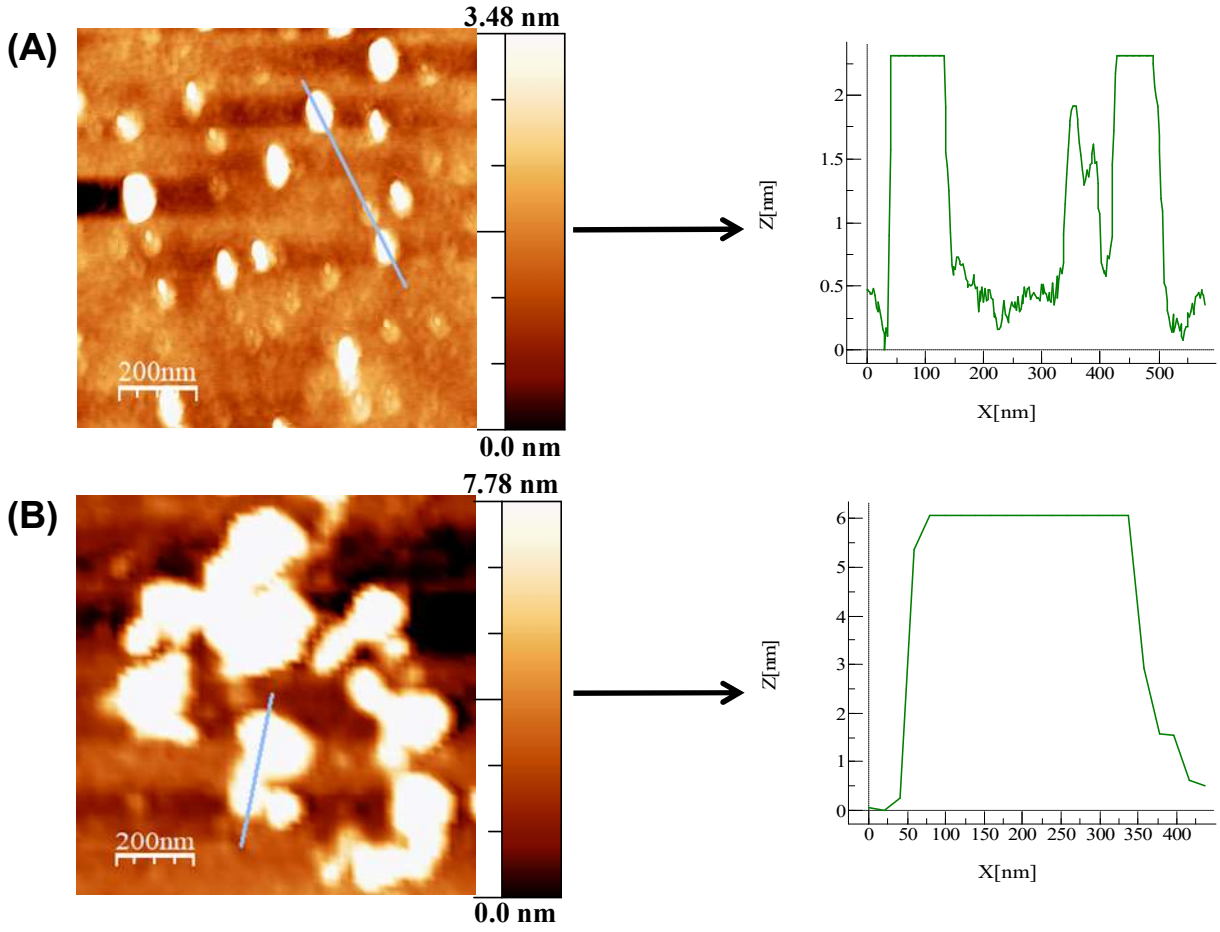

Figure S7:AFM micrograms of (A) MG-1 and (B) MG-2 with the height profile graph

Table S5 Elemental composition of PP-1 and PP-2

S.R No.	Samples	Experimental elemental composition		
		C%	N%	H%
1.	PP-1	43.9	16.83	7.17
2.	PP-2	50.30	16.09	8.01

Table S6 Zeta potential of microgels and porous polymers

Samples	Zeta potential for Micro-gel[mV]	Zeta potential for porous polymers [mV]
1	24.6	39.4
2	31.8	63.1

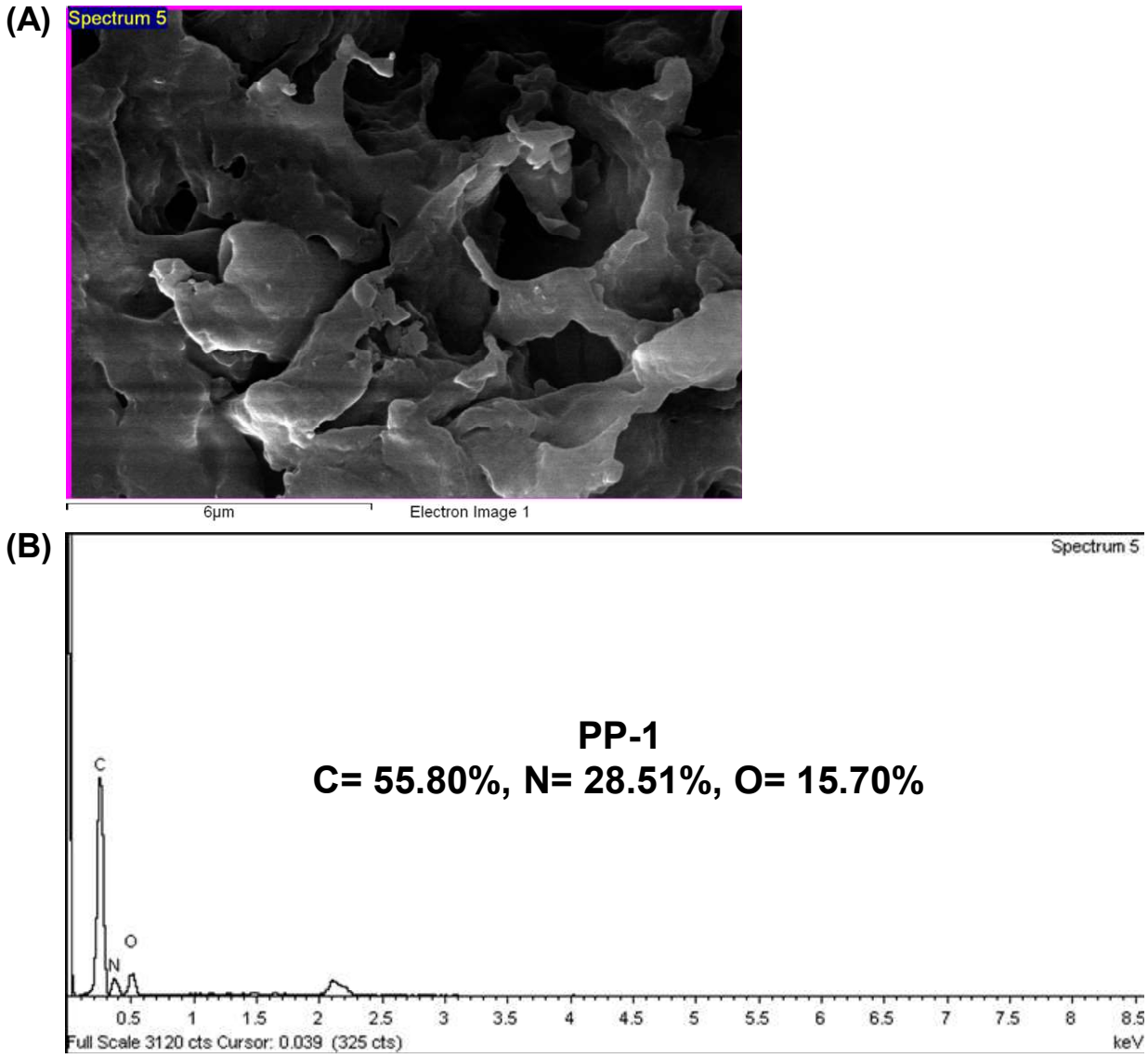

Figure S8: (A)SEM micrograph of PP-1 (B) EDX Line Spectra of PP-1

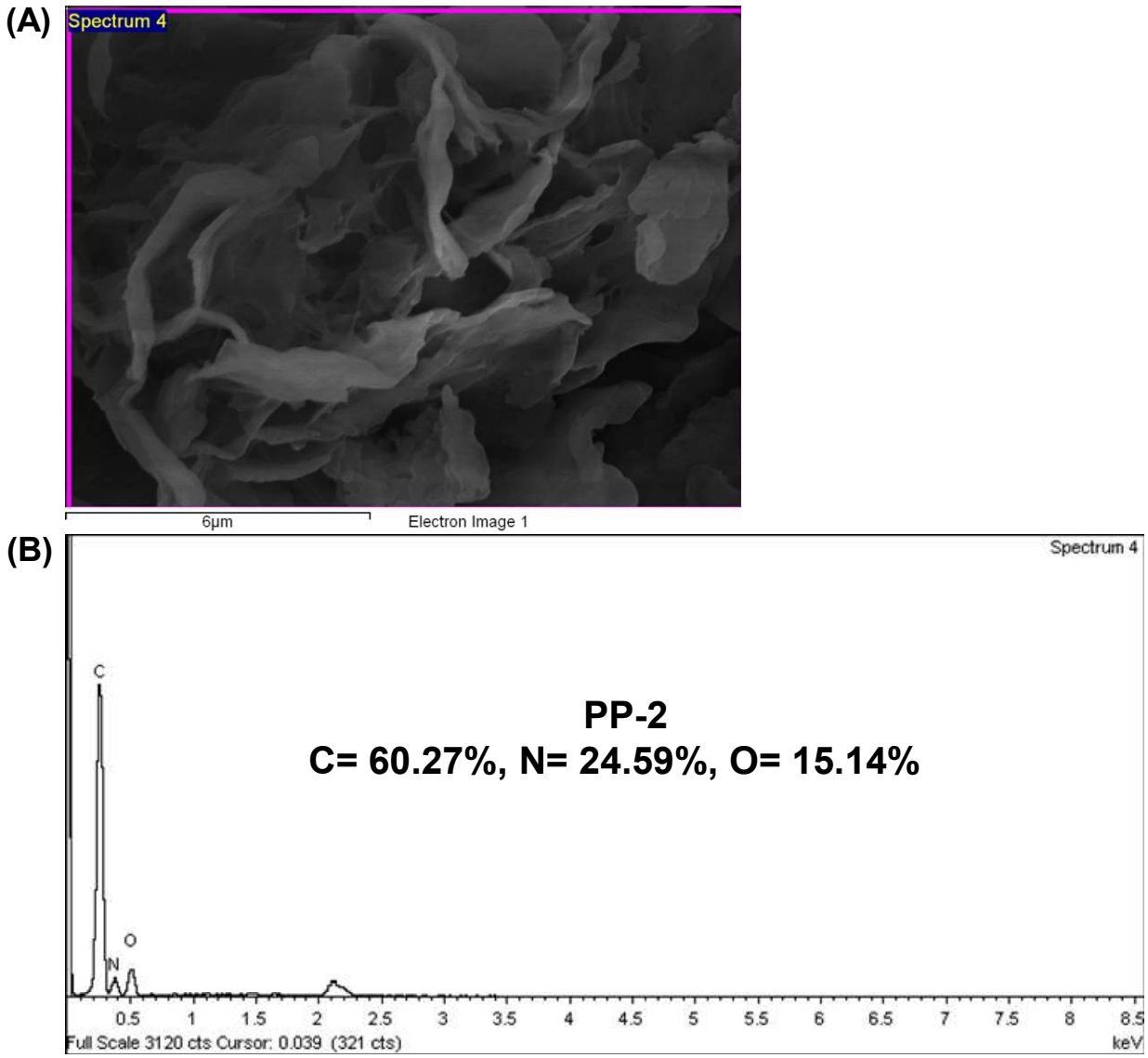

Figure S9: (A)SEM micrograph of PP-2 (B) EDX Line Spectra of PP-2

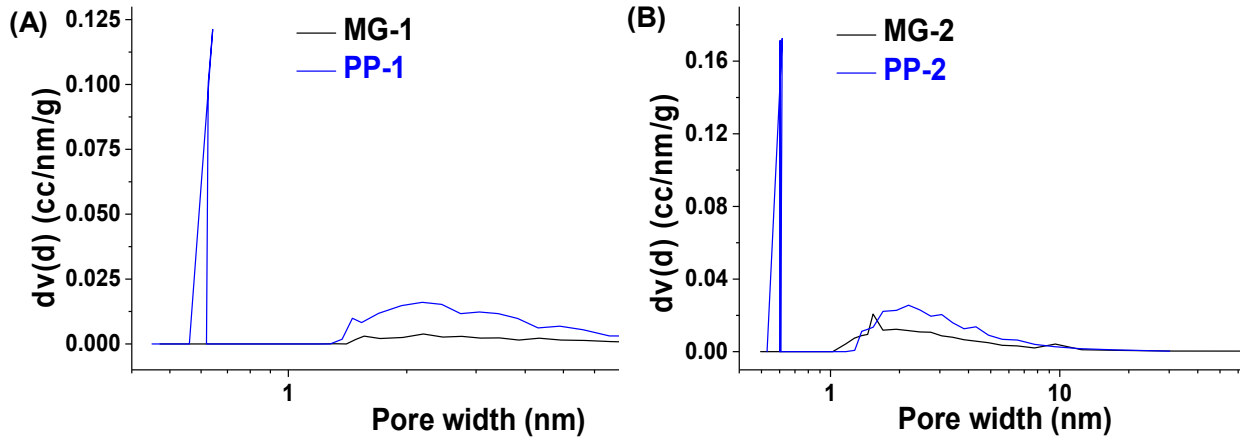

Figure S10: Comparing the pore size distribution (By BJH method) of porous polymers and corresponding microgels (A) MG-1 and PP-1 and (B) MG-2 and PP-2

Table S7 Porosity parameter of PP-1 and PP-2

Samples	Total Pore Volume ($V_{1.0}$, NLDFT)	Total Pore Volume ($V_{1.0}$, BJH)	Average Pore size (NLDFT)	Average Pore size (BJH)
PP-1	0.049 cc/g	0.072 cc/g	1.78 nm	0.64 nm
PP-2	0.082 cc/g	0.118 cc/g	1.78 nm	0.61 nm

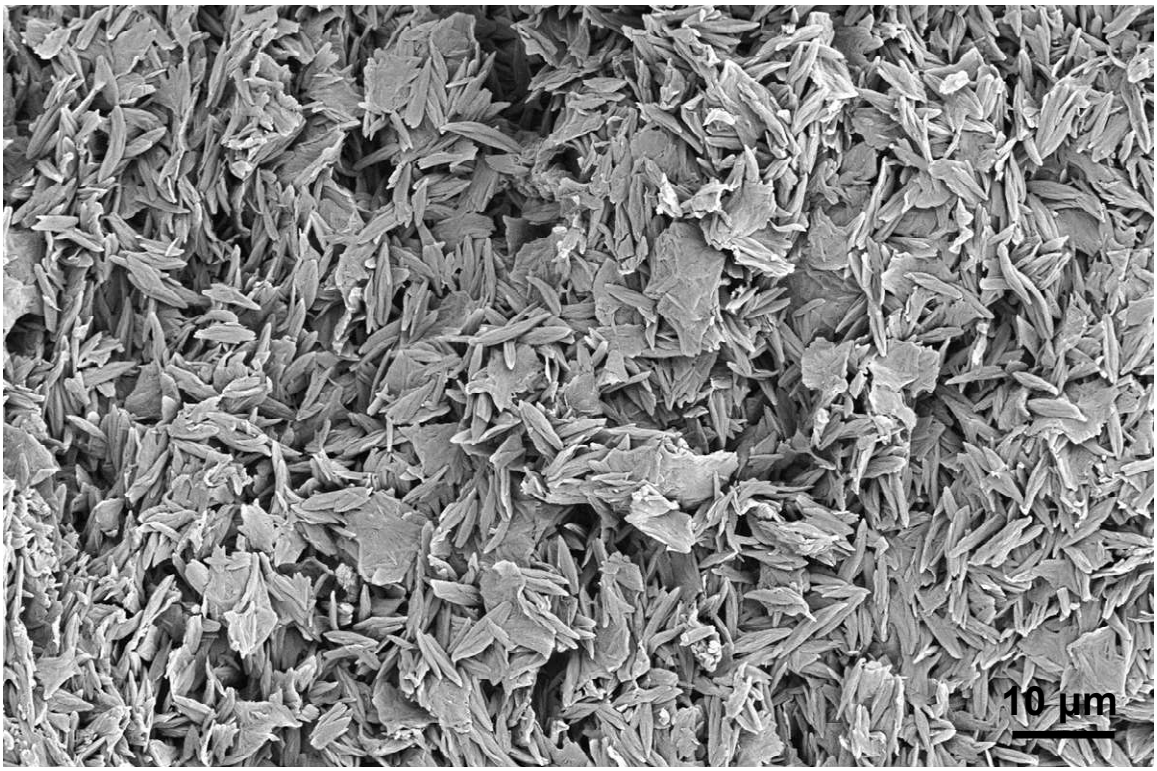

Figure S11: SEM micrograph of porous polymer (PP- 2a)using (H_2O:DMF) as reaction solvent

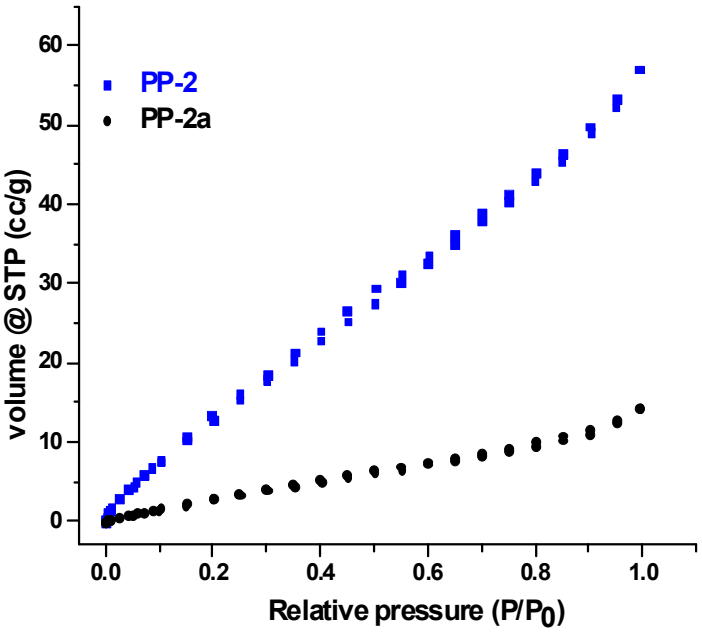

Figure S12: N_2 adsorption-desorption isotherm of PP-2 and PP-2a

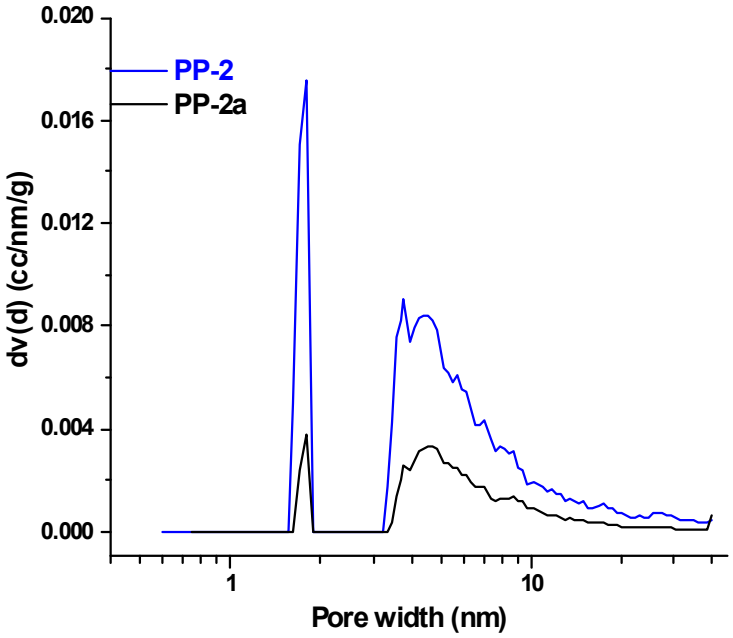

Figure S13: Pore size distribution of the PP-2 and PP-2a polymers calculated by NLDFT method

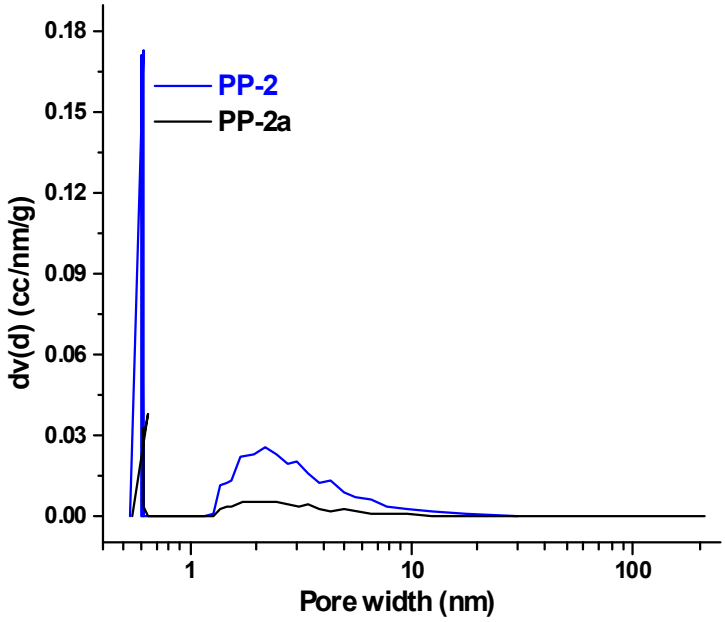

Figure S14: Pore size distribution of the PP-2 and PP-2a polymers calculated by BJH method

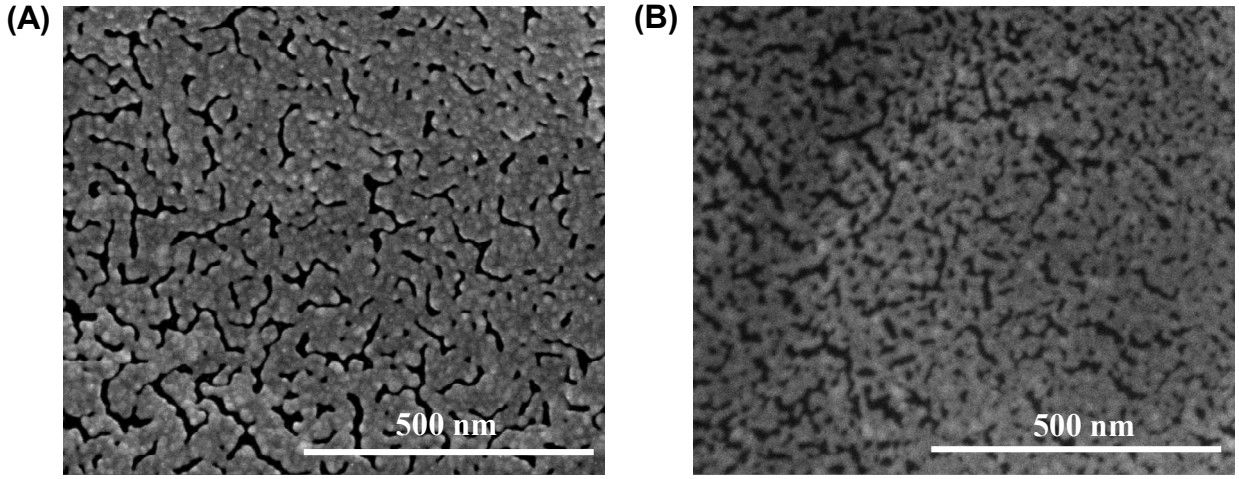

Figure S15:SEM analysis of the coated silicon wafer microgram of porous coated surfaces (A) using MG-1 and (B) using MG-2

Table S8 Comparison of the current work with recent literatures in context of CO_2 adsorption capacity (the best example [in context of CO_2 adsorption capacity] from the given reference was taken for comparison).

Polymers (as named in the ref paper)	S_{BET} ($m^2\ g^{-1}$)	CO_2 Uptake (mg/g)	Selectivity CO_2/N_2 CO_2/CH_4	References
NAN-2	56	65.58	72.7 (IAST) NA	Ref-1
HCPMAAM-2	142	63.81	53 (IAST) NA	Ref-2
MTPA	481	126.30	19.7 NA	Ref-3
TBP-4	80	61	49 9	Ref-4
HCPMAAM-1	298	68.65	86 – 45 (IAST) NA	Ref-5
PP-2	75.09	81.25	22.54 49.08	This work

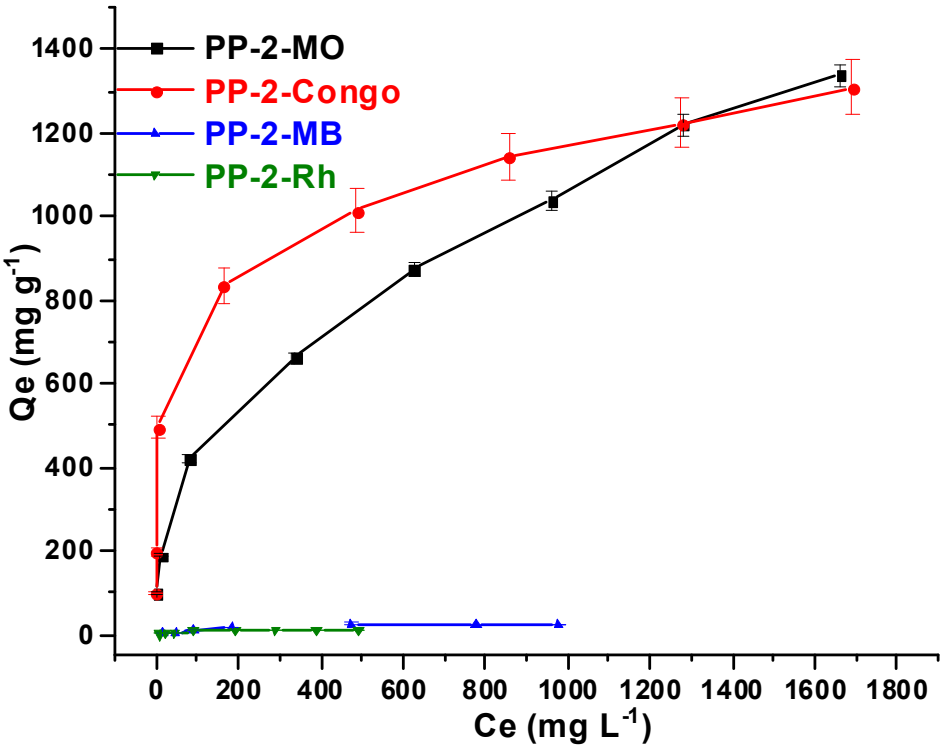

Figure S16: Equilibrium adsorption isotherms of methyl orange, congo red, methylene blue and rhodamine B dyes onto PP-2

Adsorption isotherm models- The Langmuir and Freundlich isotherm model were employed to examine the adsorption isotherm behavior of the PP-1 and PP-2 for the iodine, methyl orange and congo red.

The Langmuir isotherm model-The Langmuir isotherm is presented by the following equation (1)

$$Q_e = Q_m K_L C_e/(1+K_L C_e) \quad \text{.....(1)}$$

Where Ce (mg L-1) is iodine and dyes concentration at equilibrium, Qe (mg g-1) denote the equilibrium adsorption capacity. Q_m (mg g-1) is the maximum adsorption capacity of PP-1 and PP-2 for iodine and dyes and K_L (mg L^{-1}) is Langmuir adsorption constant that demonstrate binding energy of adsorption

The Freundlich isotherm model- The Freundlich isotherm model described by the following equation (2)

$$Q_e = K_F C_e^{1/n} \quad \text{.....(2)}$$

Where C_e (mg L-1) is iodine and dyes concentration at equilibrium, Q_e (mg g-1) denote the equilibrium adsorption capacity $K_F$and n are the adsorption capacity and the adsorption intensity constant for Freundlich adsorption isotherm model.

Table S9 Adsorption Isotherm Parameters of the Langmuir and Freundlich Model for MO removal by PP-1 and PP-2

		Langmuir model			Freundlich model		
Polymers	Adsorbate	Q_m (mg g−1)	K_L(L mg−1)	R^2	K_F (L mg−1)	n	R^2
PP-1	MO	491.81	0.003	0.963	36.05	3.021	0.970
PP-2	MO	1571.37	0.0024	0.941	66.272	2.475	0.996

Table S10 Adsorption Isotherm Parameters of the Langmuir and Freundlich Model for congo red removal by PP-1 and PP-2

		Langmuir model			Freundlich model		
Polymers	Adsorbate	Q_m (mg g−1)	K_L (L mg−1)	R^2	K_F (L mg−1)	n	R^2
PP-1	Congo red	1317.32	0.009	0.974	170.52	3.60	0.948
PP-2	Congo red	1124.80	0.151	0.906	270.14	4.68	0.977

Table S11 Adsorption Isotherm Parameters of the Langmuir and FreundlichModel for iodine removal by PP-1 and PP-2

		Langmuir model			Freundlich model		
Polymers	Adsorbate	Q_m (mg g−1)	K_L (L mg−1)	R^2	K_F (L mg−1)	n	R^2
PP-1	Iodine	2020.42	0.005	0.905	286.98	4.07	0.946
PP-2	Iodine	3020.59	0.046	0.955	661.64	4.47	0.895

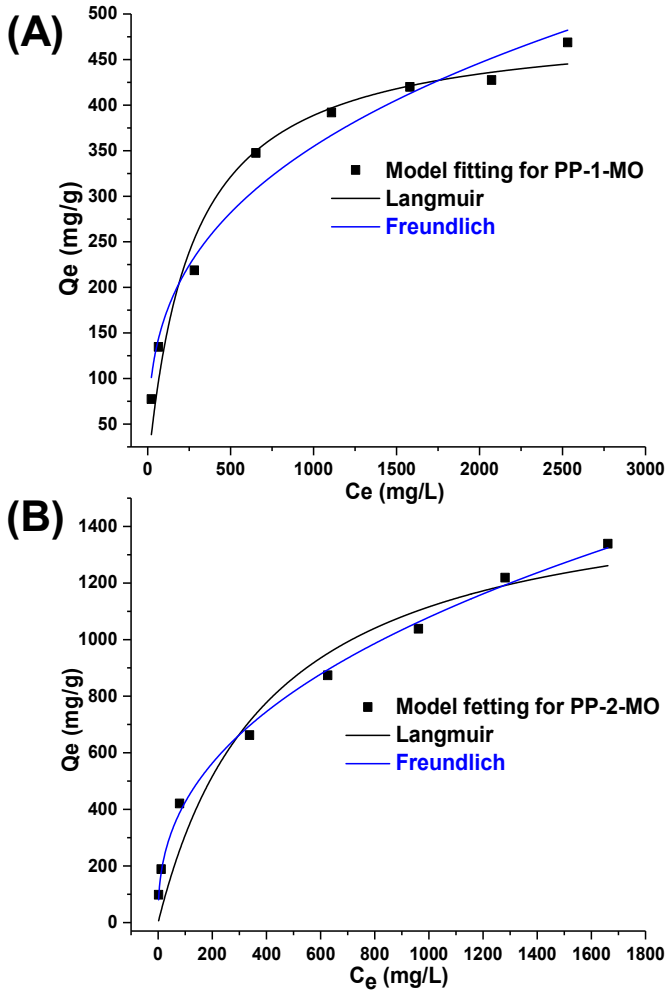

Figure S17: Langmuir and Freundlichadsorption isotherm models for MO, removal by (A) PP-1 and (B) PP-2

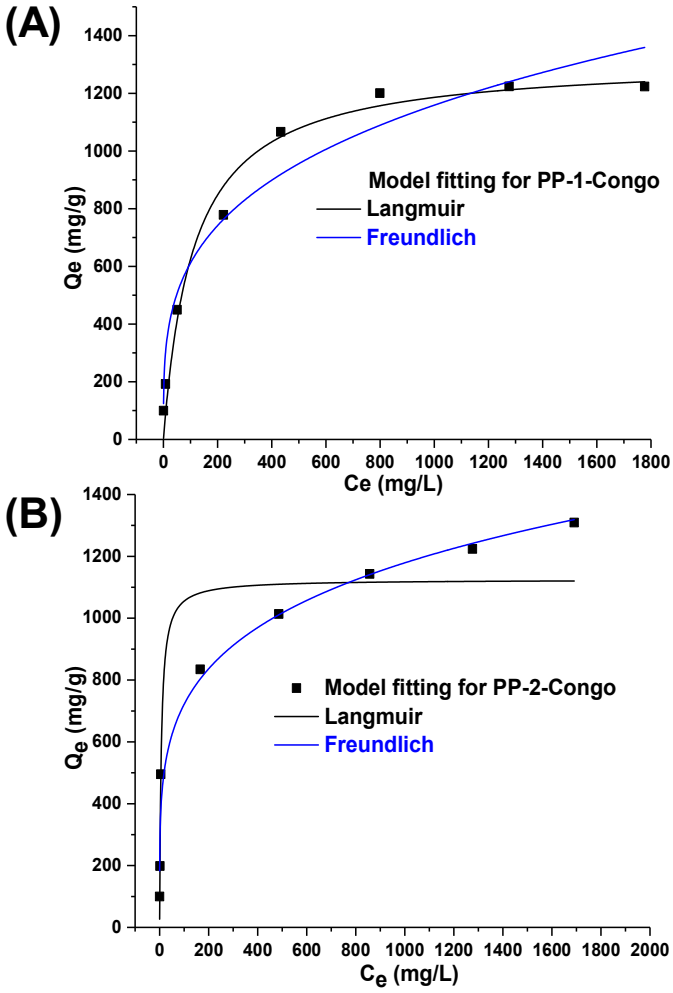

Figure S18: Langmuir and Freundlichadsorption isotherm models for congo red, removal by (A) PP-1 and (B) PP-2

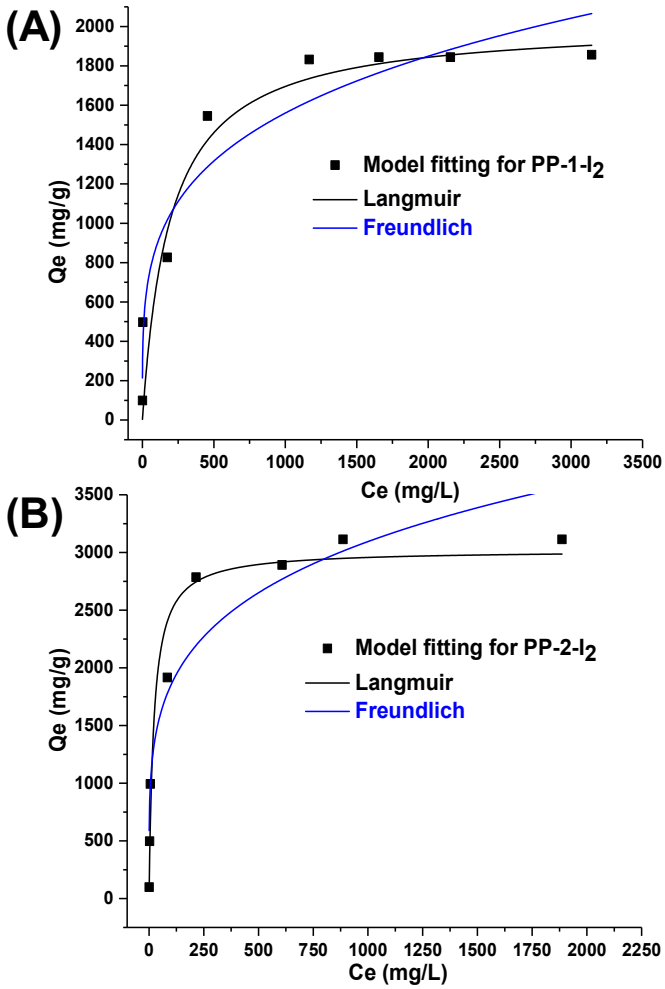

Figure S19: Langmuir and Freundlichadsorption isotherm models for iodine, removal by (A) PP-1 and (B) PP-2

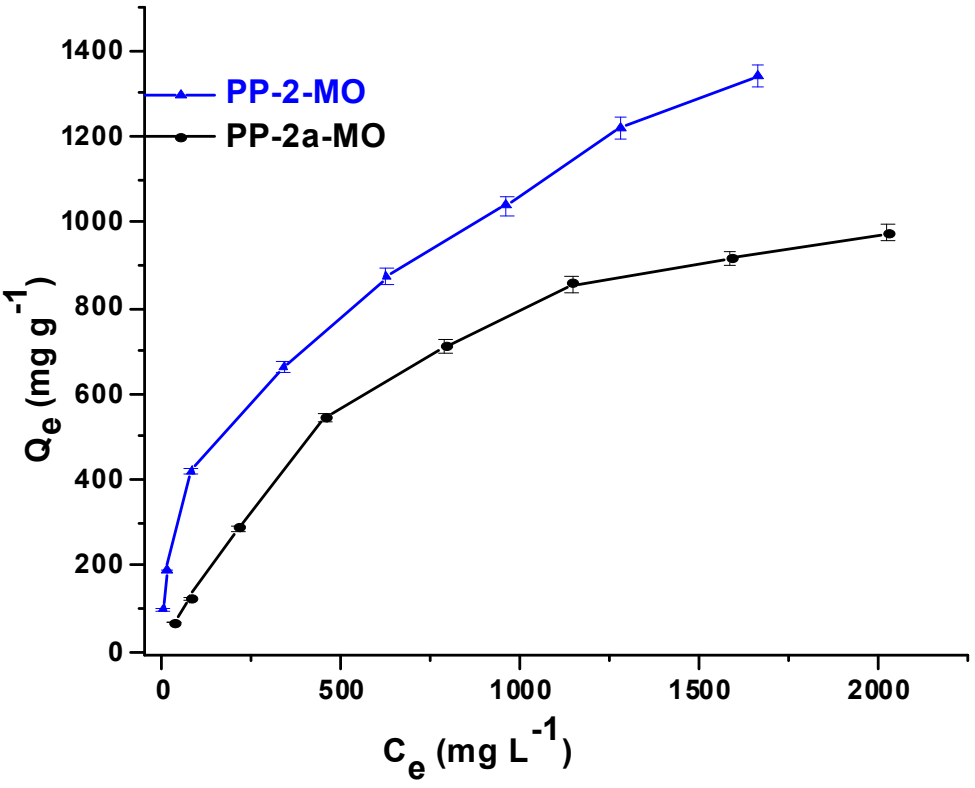

Figure S20: Equilibrium adsorption isotherms of methyl orange onto PP-2 and PP-2a

Table S12 Comparison of the current work with recent literatures in context of dye adsorption capacity (the best example from the given reference was taken for comparison).

Adsorbent	Dye	S_{BET} (m^2 g^{-1})	Dyes adsorption capacity (mg/g)	References
C-NSANaphHCP@Br	Methyl orange Methylene blue Rhodamine B	788	1010 mg g^{-1} 824 mg g^{-1} 142 mg g^{-1}	Ref-6
PMOP	Methylene blue Congo red	1604	394 mg g^{-1} 932 mg g^{-1}	Ref-7
Viologen-basedβ-cyclodextrin polymer (V-CDP)	Congo red Methyl orange	22	323 mg g^{-1} 370 mg g^{-1}	Ref-8
CrosSlinked chitosan/βcyclodextrincomposit (CRCSCD)	Methyl orange	NA	392 mg g^{-1}	Ref-9
Hybrid porous materials (HPPs)	Rhodamine B Congo red Crystal violet Methylene blue Methyl orange	862	1666 mg g^{-1} 1040 mg g^{-1} 862 mg g^{-1} 144 mg g^{-1} 67 mg g^{-1}	Ref-10
PFCMP-0	Congo red	901	1376.7 mg g^{-1}	Ref-11
MOP-2	Methylene blue	327	1153 mg g^{-1}	Ref-12
PP-2	Methyl orange Congo red	75.09	1571.3 mg g^{-1} 1124.8 mg g^{-1}	This work

Table S13 Comparison of the current work with recent literatures in context of iodine adsorption capacity in solution (the best example from the given reference was taken for comparison).

Adsorbents	S_{BET} (m^2 g^{-1})	Adsorption capacity (mg/g)	References
SCMP-2	855	249.07	Ref-13
CSU-CPOPS2	554.8	374.12	Ref-14
NRPP-2	1028	505.05	Ref-15
AzoPPN	400	735.64	Ref-16
FCMP-600@2	636	729	Ref-17
PP-2	75.09	3020.59	This work

Adsorption kinetic studies -

The pseudo-first-order kinetic model-The pseudo-first-order kinetic model is presented by the following linear equation (3)

$$\ln (q_e - q_t) = \ln q_e - k_1 t \quad \ldots\ldots\ldots\ldots (3)$$

Where $q_t$andq_e are the amount of dyes and iodine adsorbed at equilibrium and time t, k_1 (min^{-1}) is the rate constant of linear pseudo-first-order model for adsorption kinetic behavior

The pseudo-second-order kinetic model-The pseudo-second-order kinetic model is described by the following linear equation (4)

$$\frac{t}{q_t} = \frac{1}{k_2 q_e^{\,2}} + \frac{t}{q_e} \quad \ldots\ldots\ldots\ldots\ldots\ldots (4)$$

Where q_t and q_e are the amount of dyes and iodine adsorbed at equilibrium and time t, K_2 is the rate constant of linear pseudo-second-order model for adsorption kinetic behavior

Table S14 Pseudo-first-order and Pseudo-second-order Kinetic Parameters for the Adsorption of MO (100 mg/L) by PP-2

Model	Parameters	Values
Pseudo-first order	Q_e,exp (mg g^{-1})	98.7
	Q_e,cal (mg g^{-1})	91.7
	k_1 (min^{-1})	0.02813
	R^2	0.959
Pseudo-second order	Q_e,cal (mg g^{-1})	103.4
	k_2 (g mg−1 min^{-1})	0.0007
	R^2	0.994

Table S15 Pseudo-first-order and Pseudo-second-order Kinetic Parameters for the Adsorption of iodine(300 mg/L) by PP-2

Model	Parameters	Values
Pseudo-first order	Q_e,exp (mg g^{-1})	297.3
	Q_e,cal (mg g^{-1})	245.06
	k_1 (min^{-1})	0.10783
	R^2	0.989
Pseudo-second order	Q_e,cal (mg g^{-1})	317.4
	k_2 (g mg−1 min^{-1})	0.0009
	R^2	0.993

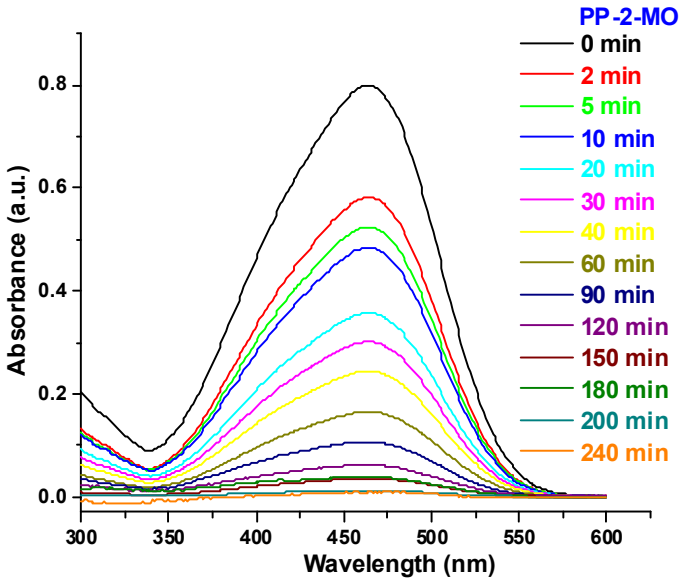

Figure S21: Kinetics study of 100 mg/L MO solutions after being treated with PP-2 by UV-Vis adsorption spectra

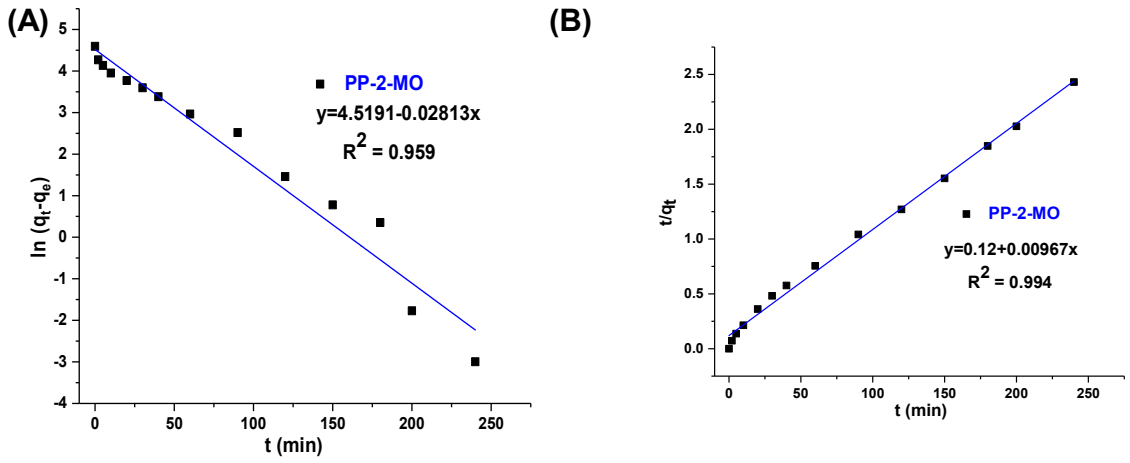

Figure S22:(A) The pseudo-first-order, (B) the pseudo-second-order kinetic model plots for adsorption of MO by PP-2

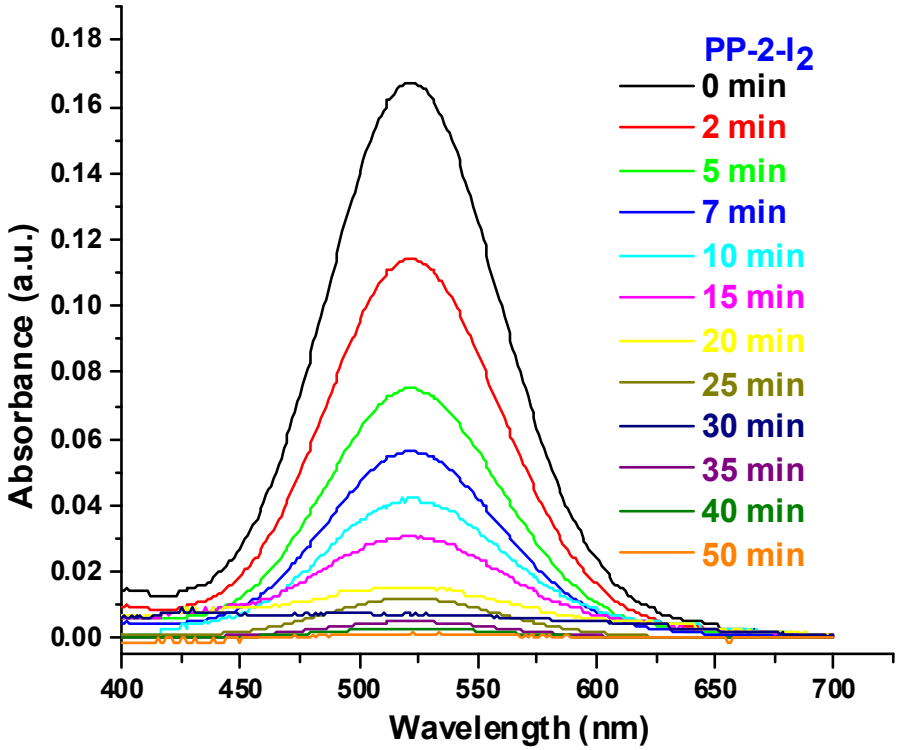

Figure S23: Kinetics study of 300 mg/L iodine solutions after being treated with PP-2 by UV-Vis adsorption spectra

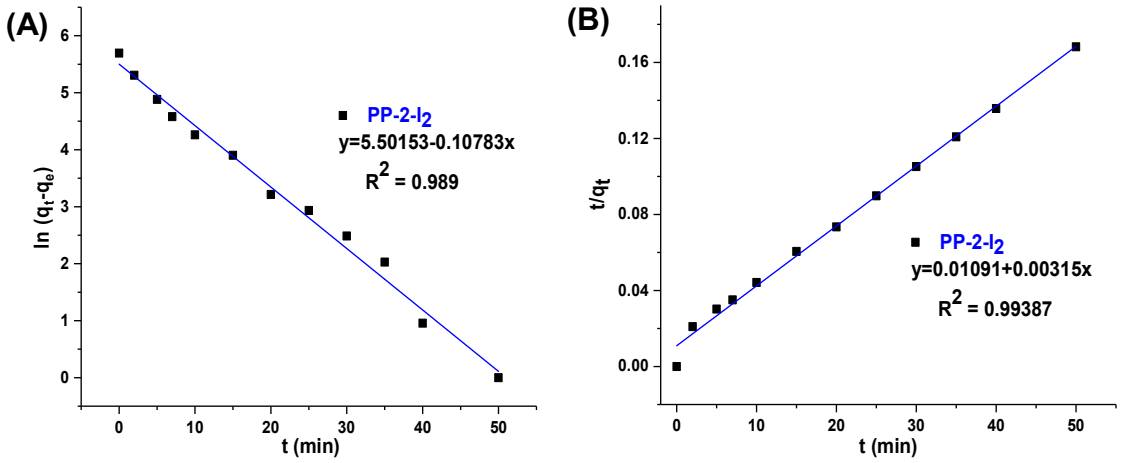

Figure S24: (A)The pseudo-first-order, (B) the pseudo-second-order kinetic model plots for adsorption of iodine by PP-2

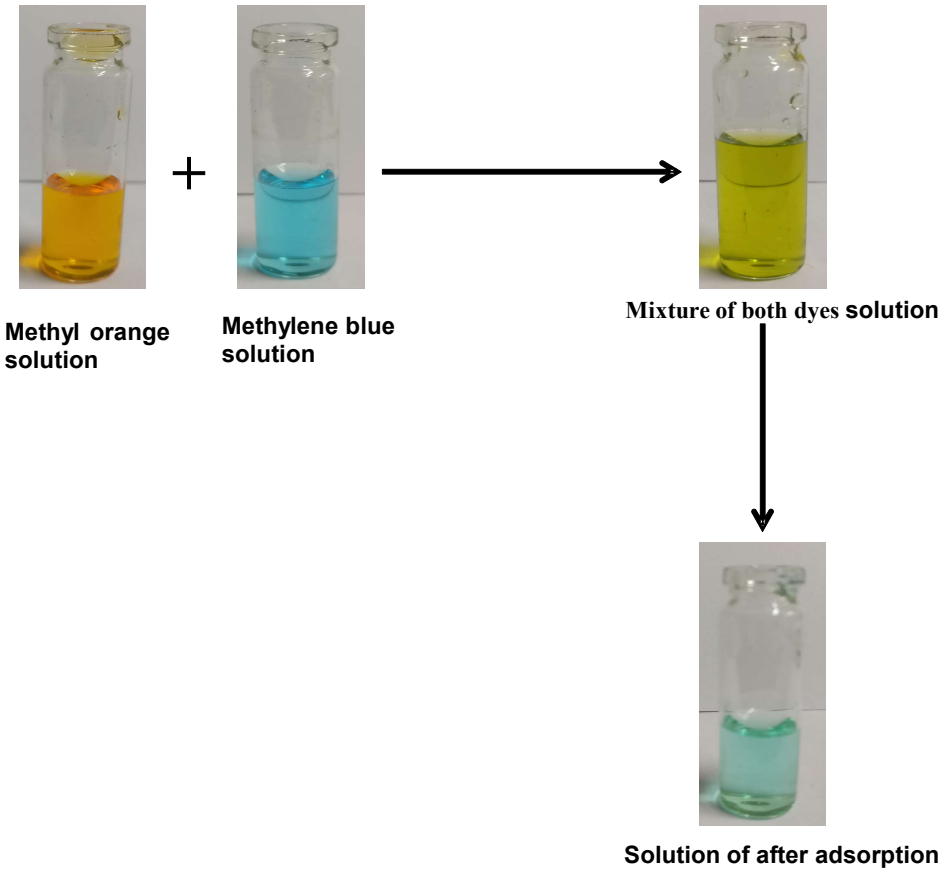

Figure S25: Photographs showing the selective adsorption of anionic (Methyl orange) dyes

(A)


S4800 10.0kV 8.9mm x6.00k SE(M)
5.00um

(B)

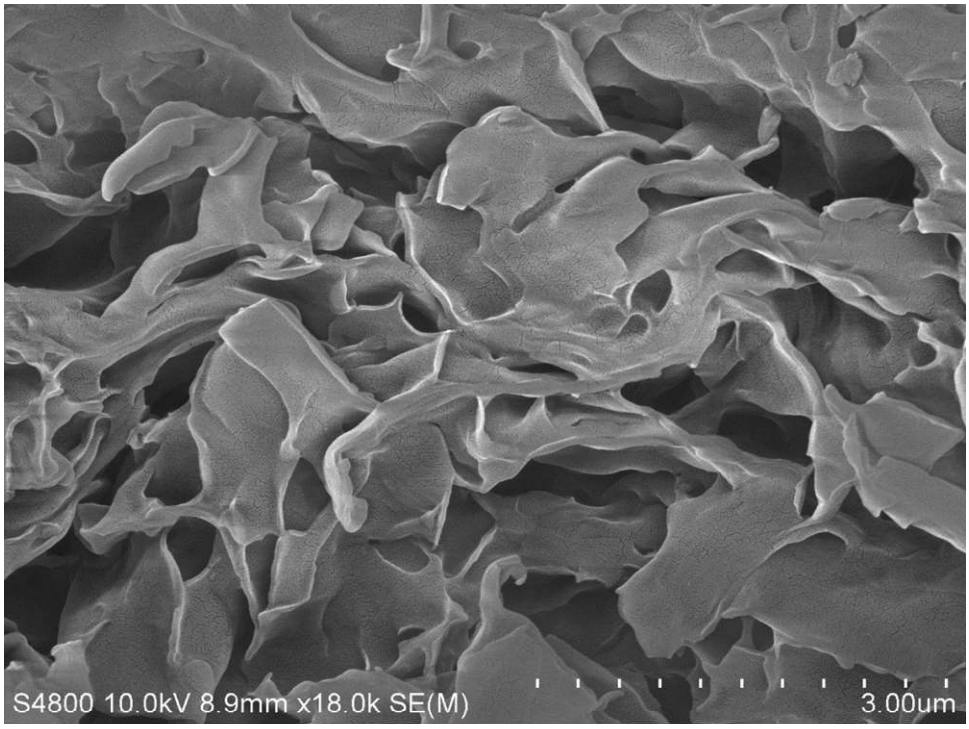
S4800 10.0kV 8.9mm x18.0k SE(M)
3.00um

(C)

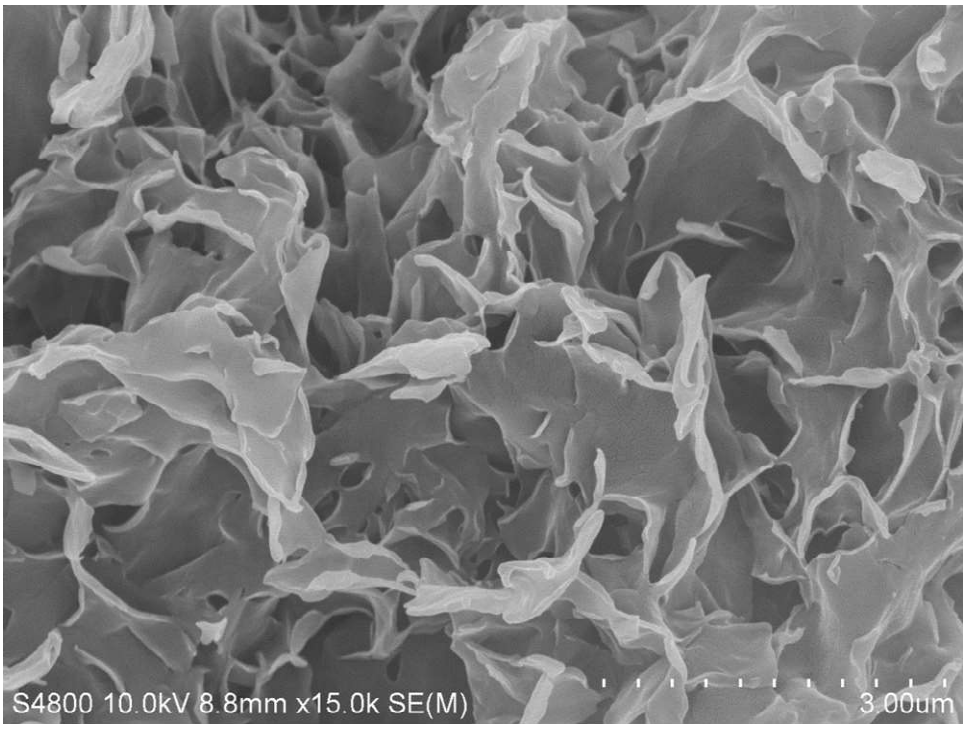

Figure S26: SEM microgram of the PP-2 (A)Before dye adsorption(B)After dye adsorption(C) After dye release

Table S16 Density calculations of microgels

MGs	M_w (g/mol)	Hydrodynamic radius (nm) (DLS)	Massof single microgels particle (g) (M_w /N_A)	Volume of microgels particle (cm^3)	Density (m/V) g/cm^3
MG-1	4.863×10^7	65.76	0.8075×10^{-16}	1.19×10^{-15}	0.06785
MG-2	8.349×10^7	165.83	1.3864×10^{-16}	1.91×10^{-14}	0.007258

The lower density indicates a more porous structure (considering similar class of materials used).

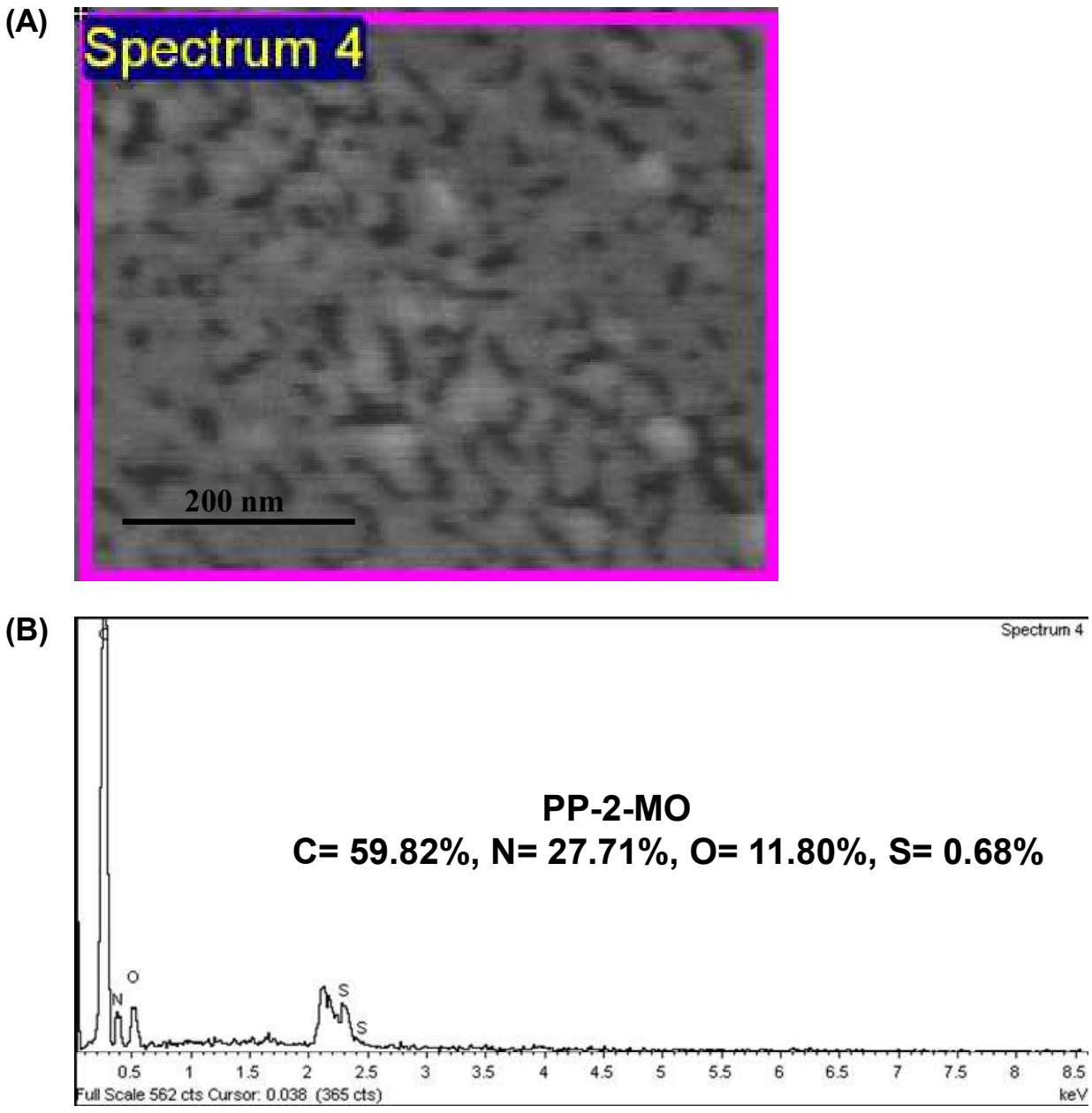

Figure S27: (A)SEM microgram of MO loaded PP-2 (B) EDX Line Spectra of PP-2-MO

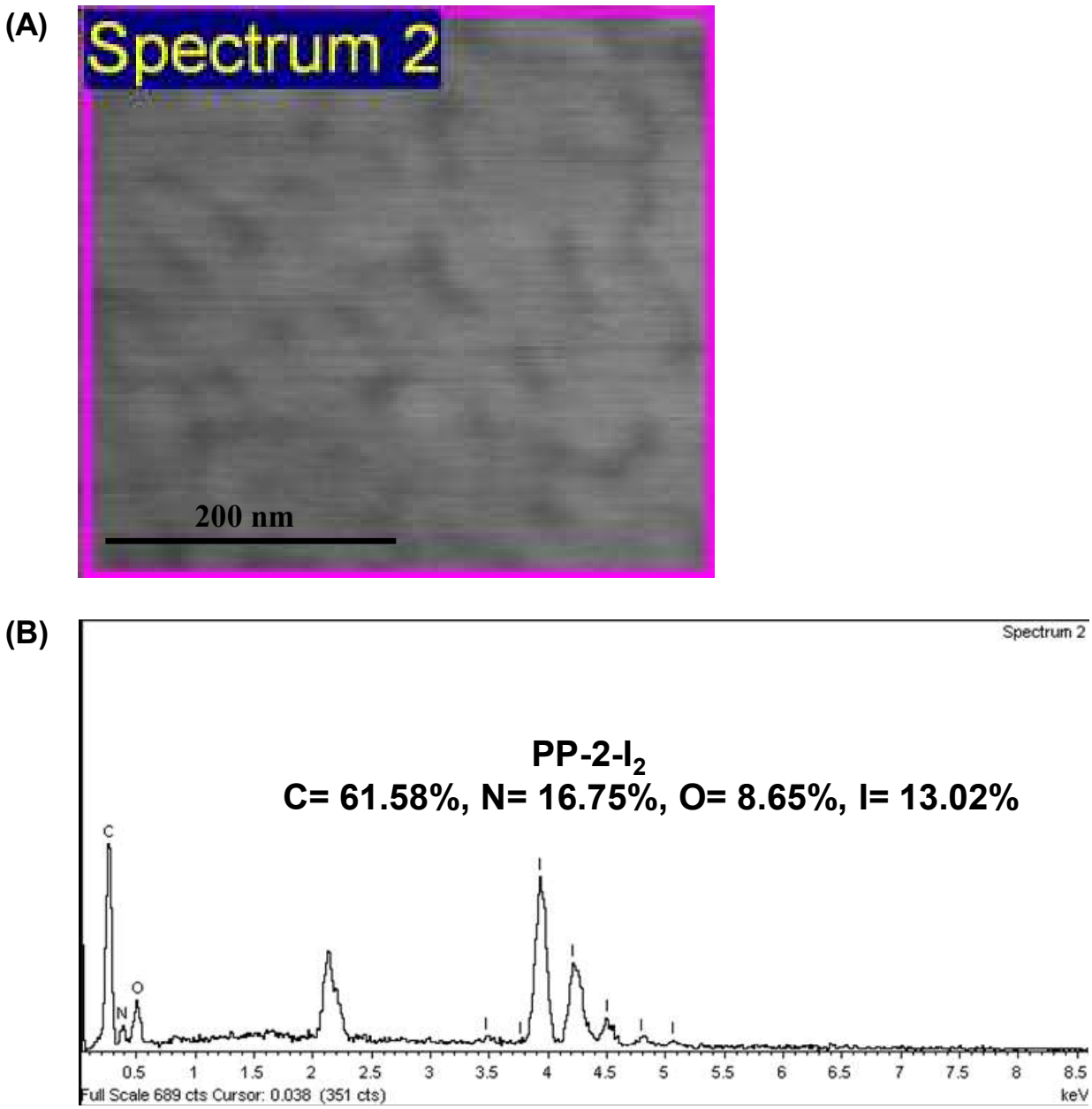

Figure S28: (A)SEM micrograph of iodine loaded PP-2 (B) EDX Line Spectra of PP-2-I_2

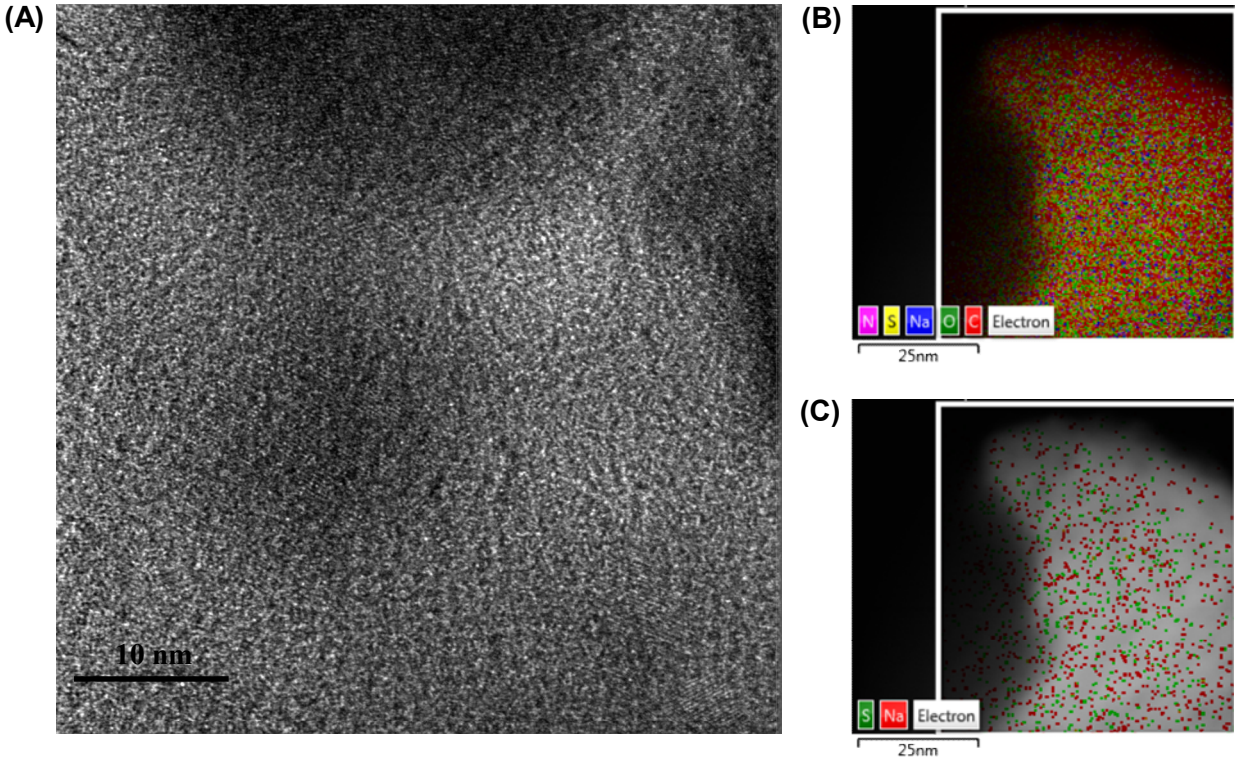

Figure S29: (A) TEM microgram of MO loaded PP-2 (B) EDX mapping for C, N, O, S and Na (C) EDX mapping for S and Na. Green and red points showing the adsorption of MO

Table S17 Adsorption Isotherm Parameters of the Zhu and Gu modelfor MO and congo red removal by PP-1 and PP-2

Zhu and Gu model							
Polymers	Adsorbate	Q_m (mg g−1)	n	K_1	K_2	K_3	R_2 value
PP-1	MO	465.32	3	0.004	$1.829\times E^{-7}$	3	0.95
PP-2	MO	1384.15	5	0.014	$1.078\times E^{-12}$	3	0.98
PP-1	Congo red	1241.15	3	0.009	$1.674\times E^{-6}$	3	0.97
PP-2	Congo red	1276.81	5	0.347	$1.355\times E^{-11}$	3	0.98

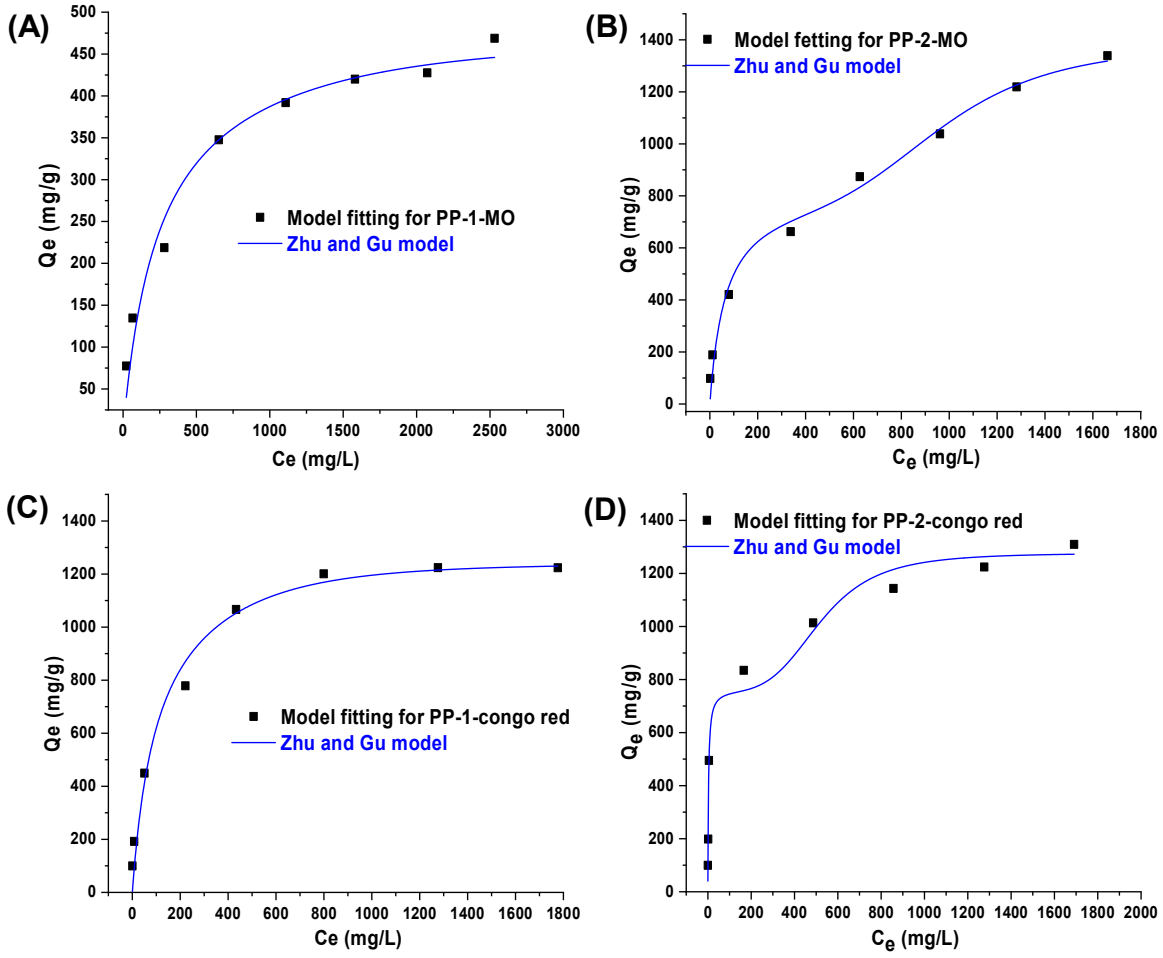

Figure S30: Zhu and Gu adsorption isotherm models for MO, removal by (A) PP-1 and (B) PP-2, and for congo red, removal by (C) PP-1 and (D) PP-2

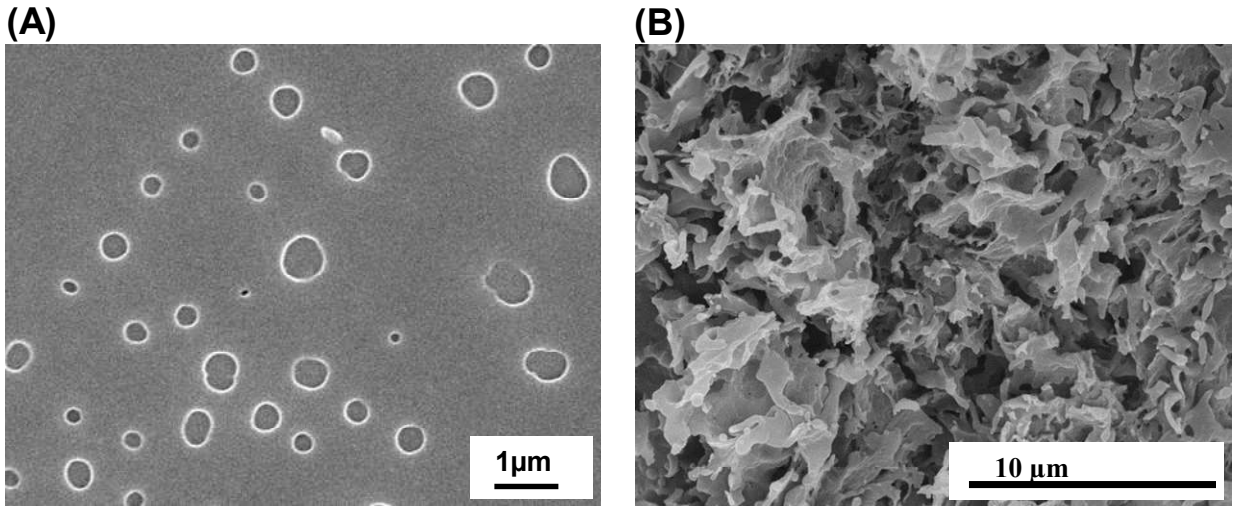

Figure S31:SEM microgram of (A) MG-1 and (B) PP-1

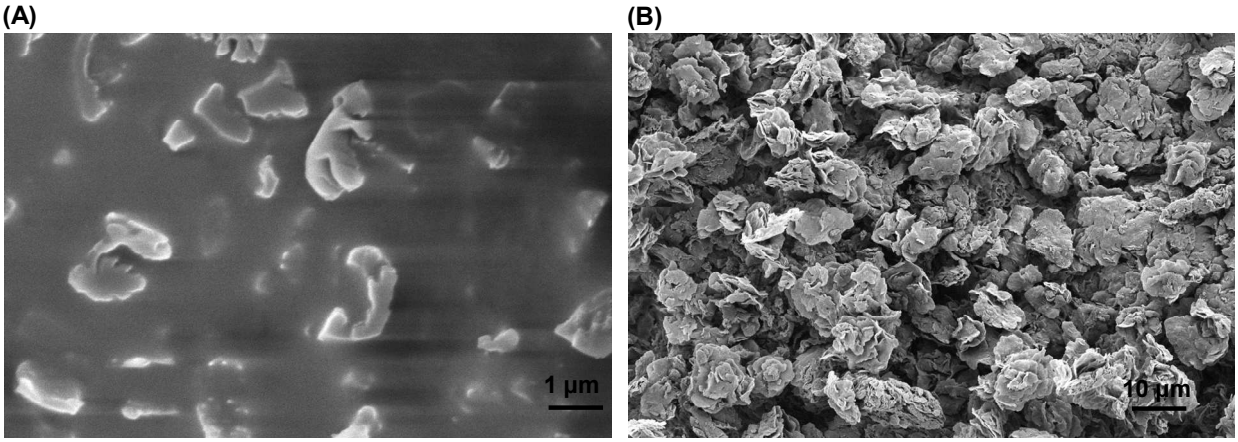

Figure S32:SEM microgram of (A) MG-2 and (B) PP-2

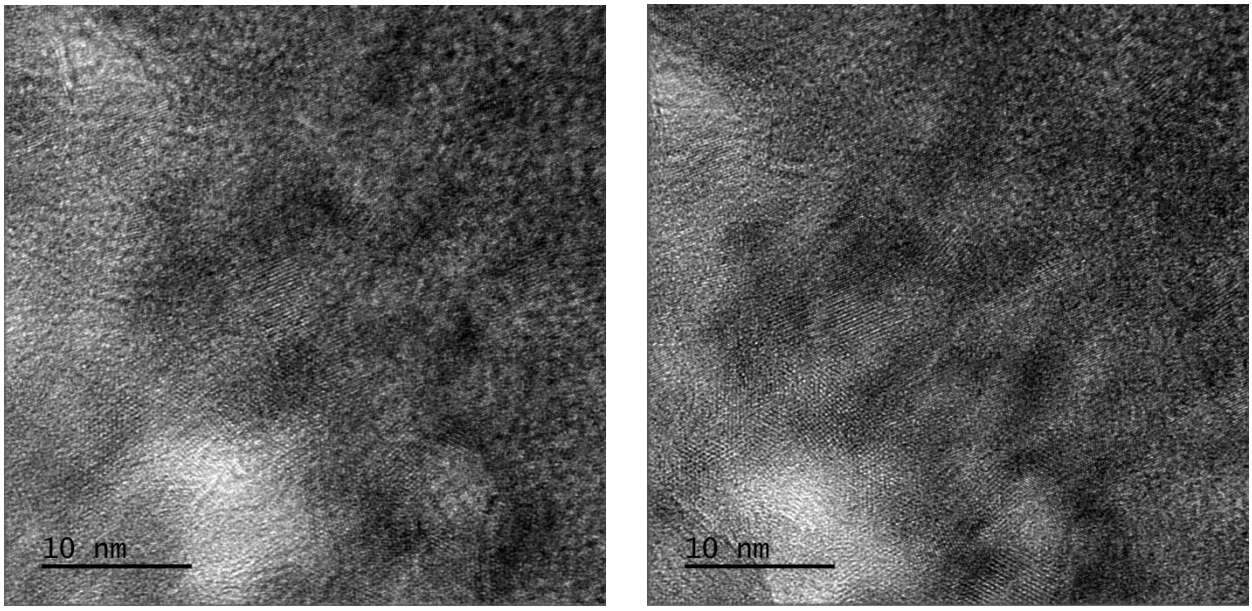

Figure S33: Additional TEM micrograms of MG-2 (collected from different regions)

References –

(1) Zulfiqar, S.; Mantione, D.; El Tall, O.; Sarwar, M. I.; Ruipérez, F.; Rothenberger, A.; Mecerreyes, D. Journal of Materials Chemistry A 2016, 4, 8190.
(2) Fayemiwo, K. A.; Chiarasumran, N.; Nabavi, S. A.; Loponov, K. N.; Manović, V.; Benyahia, B.; Vladisavljević, G. T. Industrial & Engineering Chemistry Research 2019, 58, 18160.
(3) Shao, L.; Liu, M.; Sang, Y.; Huang, J. Microporous and Mesoporous Materials 2019, 285, 105.
(4) Bera, R.; Mondal, S.; Das, N. Polymer 2017, 111, 275.
(5) Fayemiwo, K. A.; Vladisavljević, G. T.; Nabavi, S. A.; Benyahia, B.; Hanak, D. P.; Loponov, K. N.; Manović, V. Chemical Engineering Journal 2018, 334, 2004.
(6) Shen, X.; Ma, S.; Xia, H.; Shi, Z.; Mu, Y.; Liu, X. Journal of Materials Chemistry A 2018, 6, 20653.
(7) Luo, S.; Zhang, Q.; Zhang, Y.; Weaver, K. P.; Phillip, W. A.; Guo, R. ACS Applied Materials & Interfaces 2018, 10, 15174.
(8) Li, X.; Zhou, M.; Jia, J.; Jia, Q. Reactive and Functional Polymers 2018, 126, 20.
(9) Jiang, Y.; Liu, B.; Xu, J.; Pan, K.; Hou, H.; Hu, J.; Yang, J. Carbohydrate Polymers 2018, 182, 106.
(10) Liu, H.; Liu, H. Journal of Materials Chemistry A 2017, 5, 9156.
(11) Yang, R.-X.; Wang, T.-T.; Deng, W.-Q. Scientific Reports 2015, 5, 10155.
(12) Huang, L.; He, M.; Chen, B.; Cheng, Q.; Hu, B. ACS Sustainable Chemistry & Engineering 2017, 5, 4050.
(13) Qian, X.; Zhu, Z.-Q.; Sun, H.-X.; Ren, F.; Mu, P.; Liang, W.; Chen, L.; Li, A. ACS Applied Materials & Interfaces 2016, 8, 21063.

(14) Xiong, S.; Tang, X.; Pan, C.; Li, L.; Tang, J.; Yu, G. ACS Applied Materials & Interfaces 2019, 11, 27335.
(15) Abdelmoaty, Y. H.; Tessema, T.-D.; Choudhury, F. A.; El-Kadri, O. M.; El-Kaderi, H. M. ACS Applied Materials & Interfaces 2018, 10, 16049.
(16) Li, H.; Ding, X.; Han, B.-H. Chemistry – A European Journal 2016, 22, 11863.
(17) Li, G.; Yao, C.; Wang, J.; Xu, Y. Scientific Reports 2017, 7, 13972.